Tools for comprehensive reconstruction and analysis of *Drosophila* motor circuits

Anthony Azevedo[1†], Ellen Lesser[1†], Brandon Mark[1†], Jasper Phelps[2†], Leila Elabbady[1], Sumiya Kuroda[2], Anne Sustar[1], Anthony Moussa[1], Avinash Kandelwal[1], Chris J. Dallmann[1], Sweta Agrawal[1], Su-Yee J. Lee[1], Brandon Pratt[1], Andrew Cook[1], Kyobi Skutt-Kakaria[3], Stephan Gerhard[2,4], Ran Lu[5], Nico Kemnitz[5], Kisuk Lee[5,6], Akhilesh Halageri[5], Manuel Castro[5], Dodam Ih[5], Jay Gager[5], Marwan Tammam[5], Sven Dorkenwald[6,7], Forrest Collman[8], Casey Schneider-Mizell[8], Derrick Brittain[8], Chris S. Jordan[6], Michael Dickinson[3], Alexandra Pacureanu[9], H. Sebastian Seung[6,7], Thomas Macrina[5], Wei-Chung Allen Lee[2,10†††*], John C. Tuthill[1†††*]

[1]Department of Physiology and Biophysics, University of Washington, WA, USA

[2]Department of Neurobiology, Harvard Medical School, Boston, MA, USA

[3]California Institute of Technology, CA, USA

[4]UniDesign Solutions LLC, Switzerland

[5]Zetta AI, LLC, USA

[6]Princeton Neuroscience Institute, Princeton University, NJ, USA

[7]Computer Science Department, Princeton University, NJ, USA

[8]Allen Institute for Brain Science, WA, USA

[9]ESRF, The European Synchrotron, Grenoble, France

[10]F.M. Kirby Neurobiology Center, Boston Children's Hospital, Harvard Medical School, MA, USA

[†]These authors contributed equally

[††]These authors contributed equally

*Correspondence to tuthill@uw.edu, wei-chung_lee@hms.harvard.edu

Abstract

Like the vertebrate spinal cord, the insect ventral nerve cord (VNC) mediates limb sensation and motor control. Here, we applied automated tools for electron microscopy (EM) volume alignment, neuron reconstruction, and synapse prediction to create a draft connectome of the *Drosophila* VNC. To interpret the VNC connectome, it is crucial to know its relationship with the rest of the body. We therefore mapped the muscle targets of leg and wing motor neurons in the connectome by comparing their morphology to genetic driver lines, dye fills, and x-ray holographic nano-tomography volumes of the fly leg and wing. Knowing the outputs of the connectome allowed us to identify neural circuits that coordinate the wings with the middle and front legs during escape takeoff. We provide the draft VNC connectome and motor neuron atlas, along with tools for programmatic and interactive access, as community resources.

Introduction

A principal function of the nervous system is to move the body. A longstanding question in neuroscience is how neural circuits flexibly control the limbs during behaviors like walking and reaching. In vertebrate animals, enormous effort has been dedicated to understanding cortical and subcortical circuits that plan movements and issue descending commands (Arber and Costa, 2022; Inagaki et al., 2022; Leiras et al., 2022). There is also an extensive body of literature on the physiology and function of motor neurons (MNs) that directly control muscle activity (Binder et al., 2020; Kernell, 2006). In comparison, far less is known about the processing that occurs in the intermediate circuits of the spinal cord, where proprioceptive feedback signals are integrated with descending motor commands to coordinate patterns of muscle activity (Goulding, 2009; Kiehn, 2016; Ruder and Arber, 2019). For example, spinal central pattern generators (CPGs) are thought to generate rhythmic neural activity that coordinate limbs during rhythmic locomotor patterns (Rybak et al., 2015); (Grillner and Kozlov, 2021). However, understanding the architecture and activity patterns of motor circuits has been particularly challenging in mammals, due in part to the experimental inaccessibility of spinal circuits, their cell-type diversity, and the large number of spinal interneurons and motor neurons.

The adult fruit fly, *Drosophila melanogaster*, is a tractable model system to investigate neural circuits for limb motor control (Tuthill and Wilson, 2016). Leg and wing motor circuits in the fly are contained within the ventral nerve cord (VNC), which functions like the

vertebrate spinal cord to sense and move the limbs (Court et al., 2020). Each of the fly's six legs is controlled by ~70 uniquely identifiable MNs (Baek and Mann, 2009; Brierley et al., 2012; Phelps et al., 2021). For comparison, a single calf muscle in the cat is innervated by ~600 MNs (Burke, 2011).

Despite the large difference in scale, the limb motor control systems of diverse animal species possess key similarities (Manuel et al., 2019). Recent work has shown that *Drosophila* leg MNs are hierarchically recruited according to the size principle (Azevedo et al., 2020), a model formulated 50 years ago to explain relationships between MN anatomy and muscle force production in the cat leg (Henneman et al., 1965a, 1965b; Henneman and Olson, 1965; Mcphedran et al., 1965; Wuerker et al., 1965). Evidence that the size principle contributes to hierarchical MN recruitment has been found in many species, from crayfish (Hill and Cattaert, 2008) to zebrafish (Ampatzis et al., 2013) to humans (Heckman and Enoka, 2012). Thus, studying the compact motor circuits of *Drosophila* has the potential to identify circuit mechanisms that are conserved across limbed animals.

Flies have two distinct modes of locomotion: walking and flying. Unlike the leg, the *Drosophila* wing has anatomically, physiologically, and functionally distinct muscles for power and steering (Dickinson and Tu, 1997). The wing's power and steering muscles attach to the thorax and wing hinge, respectively. They are controlled by just 33 MNs; the dendritic anatomy and muscle innervation patterns of most of the wing MNs have been previously described (O'Sullivan et al., 2018). As with the leg system, the number of wing MNs is remarkably small compared with their vertebrate counterparts—a single pectoralis muscle of a hummingbird is innervated by ~2000 MNs (Donovan et al., 2012). The existence of two different locomotor control systems within the same animal creates a unique opportunity to identify general principles of motor control, as well as differences that reflect the unique demands of walking and flight.

Identifying and quantifying the synaptic inputs to MNs is an important first step in elucidating the circuit mechanisms of coordinated motor control (Arber, 2012; Kiehn, 2016). Recent advances in high-throughput serial-section EM and deep learning methods for image segmentation have dramatically accelerated the creation and analysis of massive wiring diagrams, or connectomes (Dorkenwald et al., 2022; Hulse et al., 2021). Thanks to these advances, multiple draft connectomes also currently exist for the adult *Drosophila* brain, in various states of reconstruction (Galili et al., 2022). However, the field currently lacks a connectome of the adult *Drosophila* VNC.

Here, we apply machine learning tools for automated neuron segmentation and synapse prediction to an EM volume of the *Drosophila* **F**emale **A**dult **N**erve **C**ord (FANC; (Phelps et al., 2021). We describe the application of new software tools for cell-type annotation, querying connectivity, and identification of genetic driver lines based on reconstructed neuronal morphology. The draft FANC connectome is already being actively proofread and analyzed by a consortium of 26 labs, modeled on the Flywire community (Dorkenwald et al., 2022). We now provide the FANC connectome and interactive tools as resources to the neuroscience community.

A fundamental limitation of existing EM datasets of the adult *Drosophila* brain and VNC is that they only capture the central nervous system; the fly's body and peripheral nervous system, including muscles and the projections of sensory neurons and MNs, were dissected away during sample preparation. The inability to reconstruct the peripheral inputs and outputs of the connectome poses a particular challenge for investigating how central circuits mediate motor control of the body. There does not currently exist a comprehensive wiring map, or "projectome" (Kasthuri and Lichtman, 2007), of MN to muscle connectivity in any limbed animal. Here, we set out to determine which MNs in the FANC connectome control which muscles. We assembled a comprehensive atlas of MNs by combining EM reconstruction, sparse genetic driver lines, and x-ray nanotomography of the fly's front leg and wing. Importantly, because the morphology of MNs is stereotyped from fly to fly, this projectome can be used to identify MNs in future datasets. Our approach of using multiple imaging modalities at different spatial scales can also be applied to map the inputs and outputs of connectomes across species.

Results

Automated reconstruction and tools for analysis of an EM volume of the fly VNC

We previously released the Female Adult Nerve Cord (FANC, pronounced "fancy") electron microscopy dataset, along with manual reconstructions of a handful of VNC neurons and synapses (Phelps et al., 2021). To accelerate efforts to map the VNC connectome, here we applied deep-learning based approaches to automatically reconstruct neurons and synaptic connections in FANC. Proper alignment of serial sections is crucial for automated segmentation and data analysis, so we first refined the alignment of FANC's image data using self-supervised convolutional neural networks (Popovych et al., 2022). We then used CNNs to segment the dataset into neurons and fragments of neurons and to predict synapse locations (**Figure 1C**; (Macrina et al., 2021)), as well as pre- and post-synaptic partners (Buhmann et al., 2020). To identify all cells intrinsic to the VNC, we detected nuclei using another CNN (**Figure 1E-F** and methods; (Lee et al., 2017; Mu et al., 2021)), which identified 17,076 putative cells. Through manual inspection, we classified 14,621 of these nuclei as neuronal (85.6%), 2,030 as glial (11.9%), and 425 as false positives (2.5%) (**Figure S1**).

The automated cell segmentation was ingested into a ChunkedGraph (Dorkenwald et al., 2022), which allowed human experts to proofread errors in the reconstructions through the web interface Neuroglancer (Maitin-Shepard et al., 2021). We imported synapse and cell body predictions into the Connectome Annotation Versioning Engine (CAVE), so that the associated cell segmentation for each annotation would be dynamically updated during proofreading (Consortium et al., 2021). This system allowed us to query the up-to-date connectivity and associated metadata, such as cell-type annotations. The suite of tools available for analysis of the FANC dataset are described in **Figure S2**, including a web platform (https://braincircuits.io) for performing color-depth MIP searches to find genetic driver lines that label any EM-reconstructed neuron (Otsuna et al., 2018). Following the example of FlyWire (Dorkenwald et al., 2022), we have organized a community effort currently comprising over 100 users from 26 labs who use these tools to proofread the FANC cell segmentation and analyze their circuits of interest.

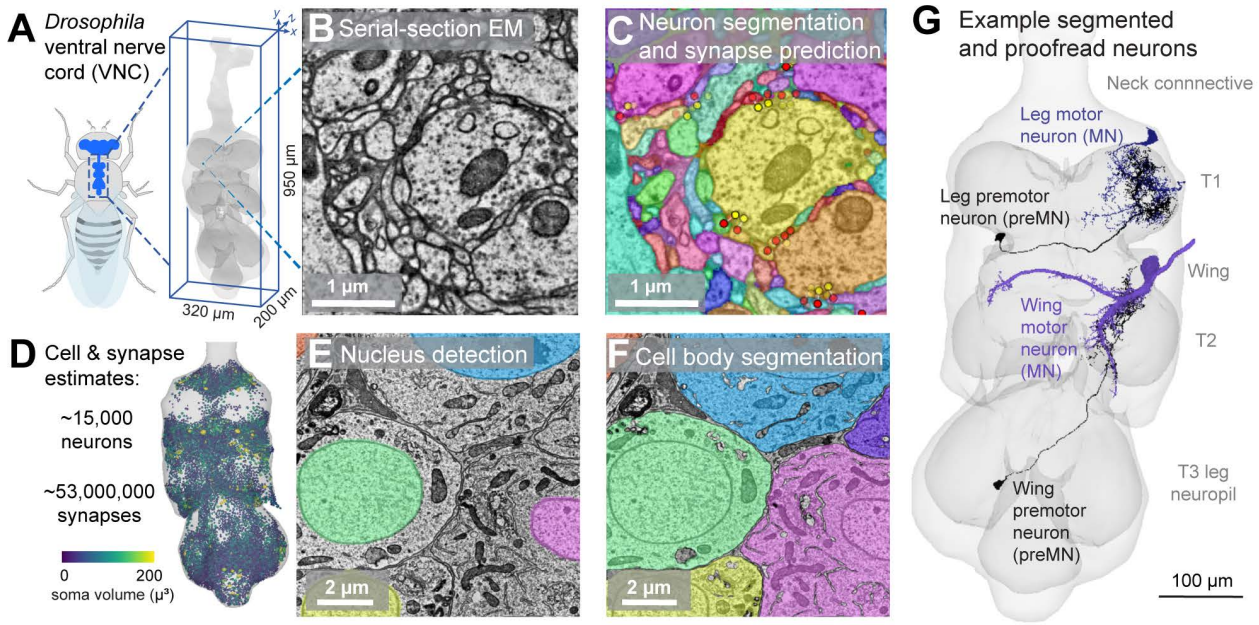

Figure 1. Automated tools for connectomic reconstruction of neural circuits in the *Drosophila* VNC. (**A**) We aligned, segmented, and analyzed a serial-section electron microscopy dataset of a *Drosophila* Female Adult ventral Nerve Cord (FANC, Phelps et al., 2021). (**B**) Example section of raw EM image data from the FANC dataset. (**C**) We automatically segmented neurons using convolutional neural nets and mean affinity agglomeration with semantic and size constraints (Macrina et al., 2021). Each segmented cell is shaded with a different color. We applied automated methods for synapse identification (Buhl et al., 2021) across the entire FANC dataset. Example presynaptic sites are labeled with yellow dots and postsynaptic sites are labeled red. (**D**) We counted the total number of neurons in FANC by automatically detecting cell nuclei (**E**) and segmenting cell bodies (**F**). (**G**) We visualized and proofread segmented cells in Neuroglancer, Google's WebGL-based viewer for volumetric data (Maitin-Shephard, 2019).

Representative examples of proofread motor and premotor neurons are shown in **Figure 1G**. (Links within the manuscript lead to 3D visualizations of reconstructed neurons). To assess the quality of the FANC automated segmentation and synapse prediction, we focused on leg MNs. As in other animals (Manuel et al., 2019), MNs are among the largest cells in the *Drosophila* nervous system (**Figure S1A-C**). The largest leg MN, the fast tibia flexor, has nearly 1 cm of total dendritic length. Manual tracing and synapse annotation of the fast tibia flexor MN took an expert tracer approximately 200 hours. For comparison, proofreading the automated reconstruction of this same MN to correct major errors in the automated segmentation took only 2 hours.

Overlaying the manual and automated reconstructions for individual MNs (**Figure 2B-C**) illustrates that the automated methods effectively captured most of the major dendritic branches and synapses. Most differences between manual tracing and automatic segmentation occurred at fine branch endpoints (**Figure 2D**). Manual and automatic synapse detection resulted in identification of similar numbers of synapses (**Figure 2E**) at similar locations (**Figure S1D-E**).

To assess how well the automatic segmentation and synapse prediction recover accurate synaptic connectivity, we computed precision and recall curves for each of the four MNs (**Figure 2F-G**). Here, precision is defined as the fraction of top predicted presynaptic partners that were identified as ground truth presynaptic partners via manual synapse annotation (**Figure 2F**). Conversely, recall is defined as the fraction of top ground truth presynaptic partners that were predicted (**Figure 2G**). For each MN, we found that the majority of top predicted partners are true partners, and that the majority of true top partners are predicted partners. Overall, this comparison provides

confidence that the automated segmentation, followed by appropriate proofreading, provides an appropriate level of accuracy for circuit analysis.

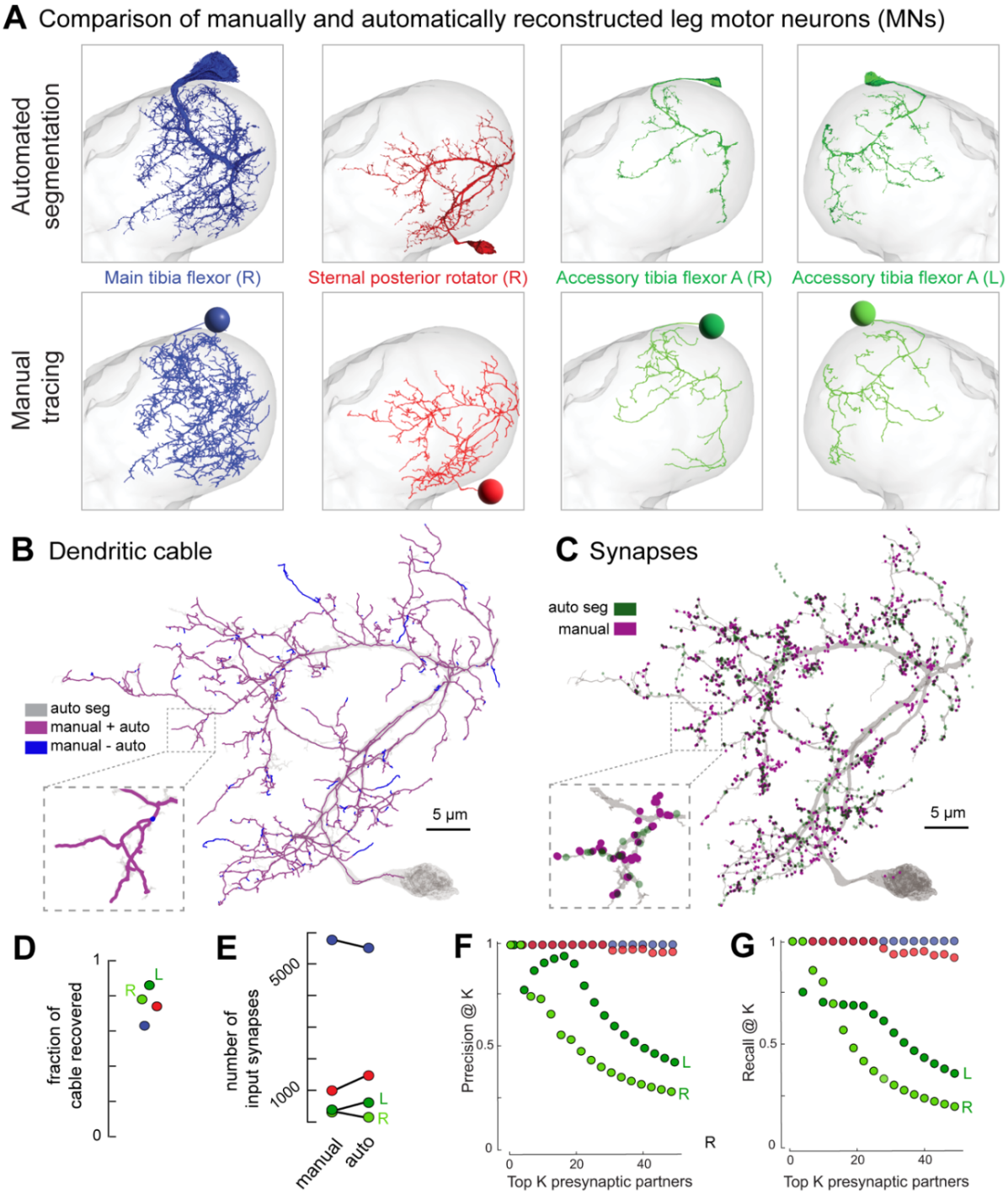

Figure 2. Validation of automated methods for segmentation and synapse prediction. (**A**) To validate the accuracy of the segmentation, we compared automated and manual reconstruction for four leg motor neurons innervating the T1 leg; three were from the right T1 neuromere (R) and one was from the left (L). Neurons were manually traced using CATMAID (Saalfeld et al., 2009). Segmented neurons were coarsely proofread in Neuroglancer without knowledge of the manual "ground-truth". (**B**) Comparison of automated and manual reconstruction for the sternal posterior rotator motor neuron. (**C**) Comparison of automated synapse prediction and manual synapse annotation for the sternal posterior rotator motor neuron. (**D**) The automated reconstruction effectively segmented most of the dendritic cable for all four motor neurons. The exceptions were typically fine dendritic branches, as illustrated in **B**. (**E**) Compared to manual annotation, the automated synapse prediction effectively identified similar numbers of input synapses for all four motor neurons. (**F**) Precision of presynaptic partners for each automatically reconstructed motor neuron. (**G**) Recall of presynaptic partners for each automatically reconstructed motor neuron.The colors indicating MN identity in **D-G** are the same as in **A**. For precision/recall analysis, we used a synapse threshold of 5 to determine the total population of synaptic partners to compare.

Identification of leg motor neurons (MNs) and target muscles

Knowing which MNs innervate which muscles is key to interpreting the connectome. We therefore set out to identify the peripheral muscle targets of all MNs innervating the fly's front (T1) leg. To reconstruct the MN projectome, we integrated information across three imaging datasets that collectively span the VNC and leg (**Figure 3A**). First, we identified and proofread all of the T1 MNs in the FANC EM dataset (69 in left T1, 70 in right T1). Second, we traced the motor nerves and axons into their target muscles using an X-ray holographic nano-tomographic (XNH) dataset of the fly's front leg (Kuan et al., 2020). Third, we screened a large collection of VNC

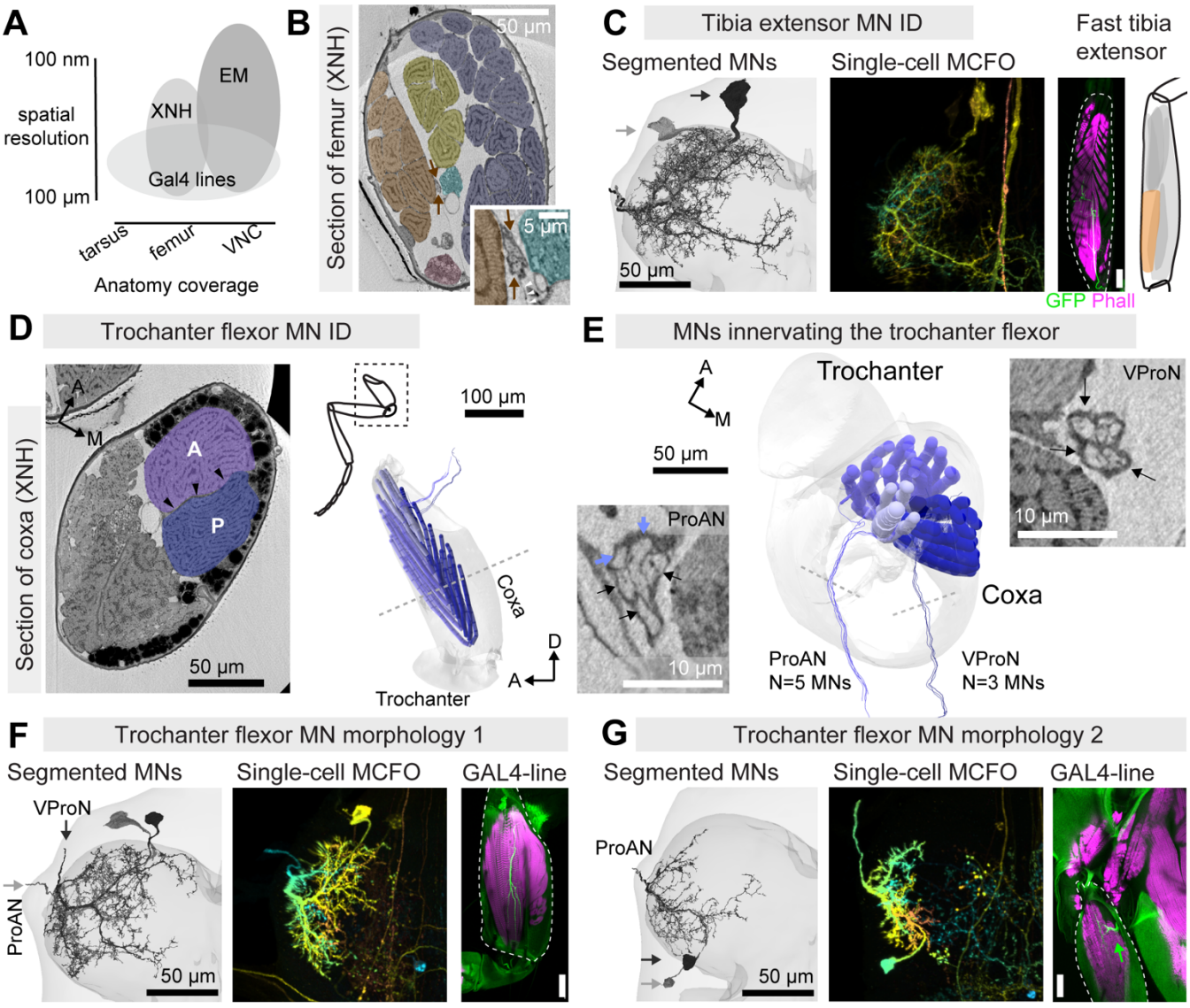

Figure 3. Matching motor neurons (MNs) in the connectome to leg muscle targets. (**A**) Schematic of spatial resolution vs. coverage of anatomical tools. (**B**) Example XNH cross-section of the femur. Orange: tibia extensor muscle fibers; blue: tibia flexor muscle fibers; yellow: long tendon muscle fibers; pink: femoral chordotonal organ. Inset: magnified view of axons (arrows) passing through a fascia membrane (arrowheads). (**C**) Identification of SETi (light) and FETi (dark) MNs. Left: tibia extensor MNs reconstructed in FANC. Center: depth-colored maximum-intensity projection (MIP) of a single MN labeled by multi-color FLP-out (MCFO; VT017399-Gal4). Right: GFP expression in the femur, driven by VT017399-Gal4 (green, projection), with phalloidin staining of the muscle (single section), schematized at right. Scale bar is 50 µm. (**D**) Left: XNH cross-section through coxa. Arrowheads indicate the extended band of the trochanter (tr.) flexor tendon. The tr. flexor tendon separates the anterior muscle fibers (light blue) from posterior fibers (dark), with proximal fibers (pale) inserting at the proximal tip of the tendon (not shown). Right: Annotated tr. flexor muscle fibers in XNH. (**E**) Projected 3D view along the long axis of the coxa. Three MNs leave the ventral prothoracic nerve (VProN) to innervate the posterior fibers (right inset). Five MNs leave the prothoracic accessory nerve (ProAN) to innervate the anterior fibers (left inset); two traced MNs in ProAN innervating proximal fibers are indicated with blue arrows. (**F**) Two of six FANC MNs with characteristic morphology, one of 3 that exit via ProAN, and one of 3 that exit via VProN. MCFO clones and GAL4-driven GFP in coxa (VT063626-Gal4). (**G**) Two FANC MNs with small posterior somas. MCFO clones and GAL4-driven GFP in coxa (VT025963-Gal4) provide evidence that at least one MN with a posterior soma innervates the proximal fibers of the trochanter flexor muscle.

neurons (Meissner et al., 2020) sparsely labeled with the multi-color Flp-out (MCFO) technique (Nern et al., 2015) to identify Gal4 driver lines (Jenett et al., 2012) labeling leg MNs. We imaged GFP expression of each genetic driver line in the front leg to identify the muscle target of each MN axon. We then compared the dendritic morphology of the genetically-labeled MNs to those reconstructed from FANC (**Figure 3**). We focused our efforts on the left MNs because the left prothoracic leg nerve (ProLN) of the FANC dataset is more intact than the right ProLN (**Figure S3**).

We illustrate the process of MN identification across the three imaging modalities with two examples (**Figure 3**). First consider the fast and slow tibia extensor MNs (**Figure 3B**, **C**) that innervate the tibia extensor muscle. These neurons have been studied extensively in other insects, where they are referred to as the FETi and SETi (Bässler and Büschges, 1998; Burrows, 1996). In the XNH volume, we identified two candidate MN axons that leave the leg nerve in the femur and pass through a membrane separating the tibia extensor muscles from the tibia flexor muscles (arrows in **Figure 3B**). We identified four GAL4 lines from the Janelia database (Jenett et al., 2012) labeling two MNs that project through the same nerve to innervate the extensor muscles. The dendritic morphology of the genetically labeled MNs closely matched the dendritic morphology of two MNs that we reconstructed in the FANC EM dataset (**Figure 3C)**. We therefore concluded that these are the FETi and SETi MNs. As in the locust (Burrows and Horridge, 1974), they can be distinguished from each other because the FETi branches more extensively than the SETi in the VNC and innervates more and larger muscle fibers in the femur. The SETi receives 7090 synaptic inputs, and the FETi receives 14,904, the most for any front leg (T1) motor neuron. The only other neuron in FANC with more synaptic inputs than the left T1 FETi is a T3 leg motor neuron with 15,474 inputs. Based on its morphology and large number of synaptic inputs, that neuron is likely the FETi for the T3 leg.

As a second example, consider the large trochanter flexor muscle in the coxa (**Figure 3D**). Compared to the SETi and FETi, little is known about the neural control or biomechanics of flexing the trochanter-femur segment to drive the insect forward during walking. The trochanter flexor tendon bisects the muscle, with anterior muscle fibers attaching to one side of the tendon and posterior fibers attaching to the other (**Figure 3D**). We traced eight MNs innervating this muscle in the XNH volume: five innervate the anterior fibers via the prothoracic accessory nerve (ProAN) and three innervate the posterior fibers via the prothoracic ventral nerve (ProVN) (**Figure 3E**). In FANC, we found six MNs with morphology that resembled previous images of trochanter flexor MNs (Enriquez et al., 2015): three that leave via the ProAN and three that leave via the ProVN (**Figure 3F**). If we assume the same number of trochanter flexor neurons exist in both FANC and XNH datasets, what about the two other MNs that innervate the muscle from the ProAN? In FANC, twelve MNs exit via the ProAN, six have somas on the posterior cortex of the neuropil, four of which likely innervate the sternal posterior rotator muscle. This left two FANC MNs in the ProAN unaccounted for (**Figure 3G**). Confocal imaging of genetic driver lines showed that at least one MN with a posterior soma innervates the proximal fibers of the trochanter flexor. From these strands of evidence, we deduced the identity of all eight MNs innervate the trochanter flexor muscle.

We applied a similar approach to identify the target muscles of all 69 left T1 MNs (**Figure 4**). A comprehensive description of leg MN identification from EM, XNH, and light-level imaging of genetic driver lines is provided in **Appendix A**. We also used the XNH dataset to determine the number of muscle fibers in each leg muscle (**Figure 4A**), along with fiber origins and cuticle attachment points. Combining this anatomical information with joint kinematics recorded from walking flies (**Figure 4B;** (Karashchuk et al., 2021) allowed us to predict which MNs contribute to distinct aspects of the step cycle, such as leg swing vs. stance (**Figure 4C)**. Importantly, because the dendritic morphology of leg MNs is stereotyped from fly to fly, this atlas (**Figure 4C-D**) can be used to identify MNs in future datasets. Indeed, it has already been used to identify MNs in a separate EM volume of the male VNC (MANC), including across different VNC segments (Cheong, Eichler et al., in preparation).

In the process of reconstructing and identifying leg MNs, we made several other observations that would have been difficult to observe without a combined approach to reconstructing neuromuscular anatomy across imaging scales (**Figure 3A**). For example, the right front leg of FANC contained 70 MNs (compared to 69 in the left T1). The extra cell appears to be a second tarsus levator MN. Supernumerary MNs have been previously described in the locust leg motor system (Siegler, 1982). Further, six MNs innervate the femur reductor muscle in the trochanter. It has been previously assumed that the *Drosophila* trochanter and femur are functionally fused (Hartenstein, 2006); however, the fact that the trochanter segment still possesses its own dedicated MNs and musculature suggests that either the two segments retain some independent biomechanical function or that the current morphology represents a palimpsest of the ancestral state.

In cases where we were able to trace MN axons to their specific target muscle fibers we found that large (fast) MNs innervate more and larger muscle fibers than small (slow) MNs (e.g. **Figures A11 and A12**). This relationship, which has also been observed in many other vertebrate and invertebrate species (Kernell, 2006; R. E. Snodgrass, 1935), is consistent with a gradient in force production across muscle fibers.

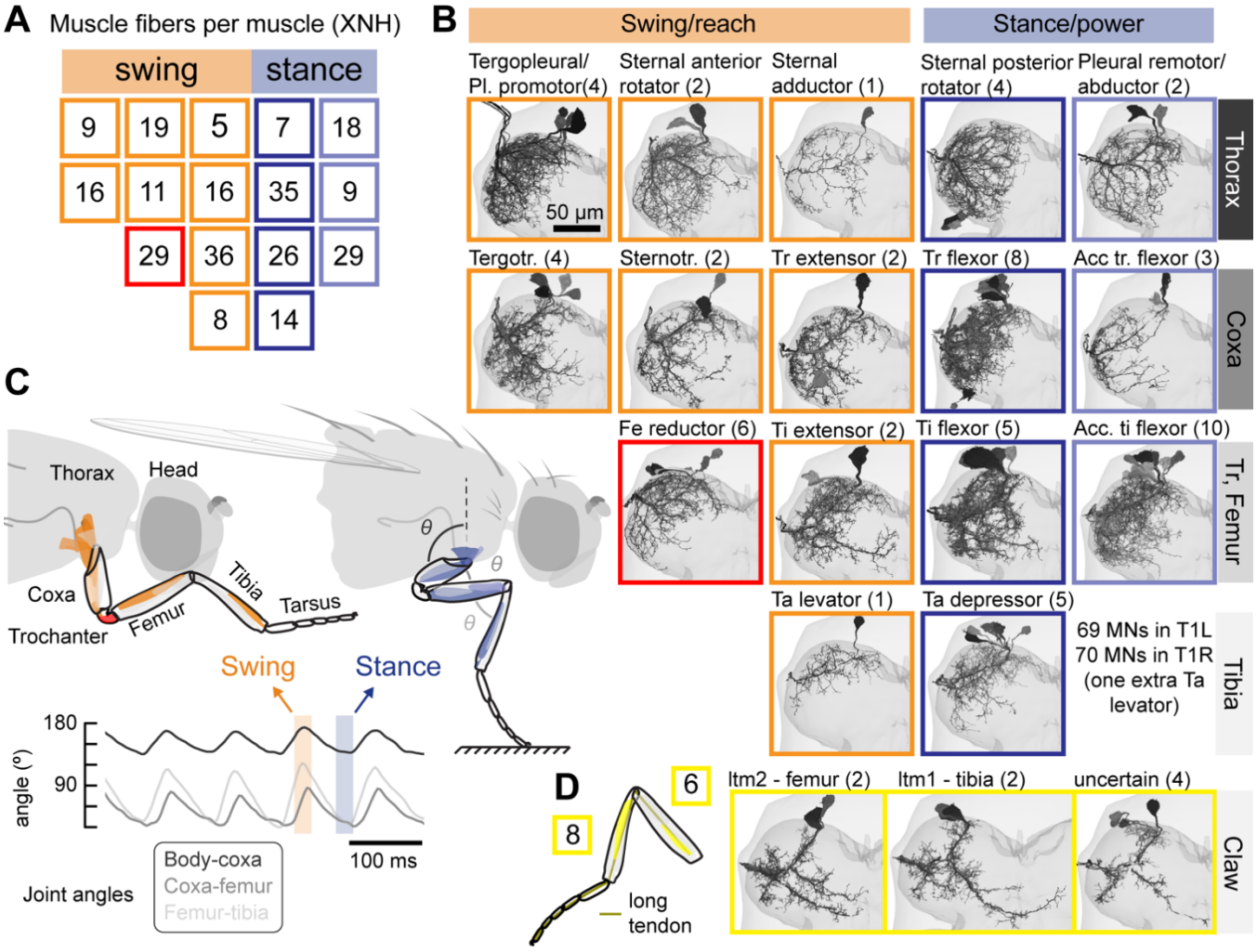

Figure 4. Identification of the specific muscle innervated by each left T1 motor neuron (MN) in FANC. (**A**) Counts of fibers in each leg muscle from XNH volume. Color code for muscles is shown in E. (**B**) Schematic of musculature, separated into muscle groups that drive the leg to swing forward or reach (orange), vs. muscles that push the fly's body forward (blue). Inset: joint angles measured from a fly walking on a spherical treadmill (Karashchuk et al., 2021). (**C**) EM-reconstructed MNs, grouped by segment (rows, labeled at right) and by muscle target (each square). Gray scale indicates different MNs, orange vs. blue indicates swing vs. stance. The femur reductor MNs that target the trochanter, whose function is unknown, are indicated by a red square. (**D**) Left: schematic of the long-tendon muscle (ltm), a multi-joint muscle with fibers in both the femur (ltm2) and tibia (ltm1) that insert onto the same long tendon (retractor unguis, dark line in the schematic) and control the tarsal claw. Left: four ltm MNs have extensive medial branches; two target ltm2, two target ltm1. The specific targets of four smaller ltm MNs are uncertain.

We found that some muscle fibers are innervated by multiple MNs, confirming that adult insect muscles can exhibit polyneuronal innervation (Hoyle, 1983). Whereas mammalian muscle fibers are often poly-innervated in neonatal animals, they are pruned during development, leading to singly-innervated fibers in adults (Brown et al., 1976). We find clear evidence from the XNH data for polyneuronal innervation in the long tendon muscle (LTM), the proximal fibers of the trochanter flexor (**Figure 4E**, not shown), and the femur reductor muscle. LTM fibers originate in both the femur (ltm2) and the tibia (ltm1), and insert on the long tendon (retractor unguis), which extends from the femur to the claw at the distal tip of the leg (**Figure 4G**, gold line) (Radnikow and Bässler, 1991). Polyneuronal innervation may endow the motor system with more flexibility and may help explain how insect limbs achieve the necessary precision despite their sparse MN innervation. Another mechanism for enhancing motor flexibility in other arthropods is the presence of GABAergic MNs that innervate many target muscles (Wolf, 2014); however, we did not find such "common inhibitor" MNs in the T1 leg.

We did not observe any presynaptic output from leg MNs in the VNC. Larval MNs innervating abdominal muscles also lack output synapses (Mark et al., 2021; Schneider-Mizell et al., 2016). This lack of output synapses is notable because the vast majority of fly neurons possess apposed input and output synapses, even in dendritic compartments. Indeed, in other arthropods, the central output synapses of MNs are essential for their role in pattern generating networks.

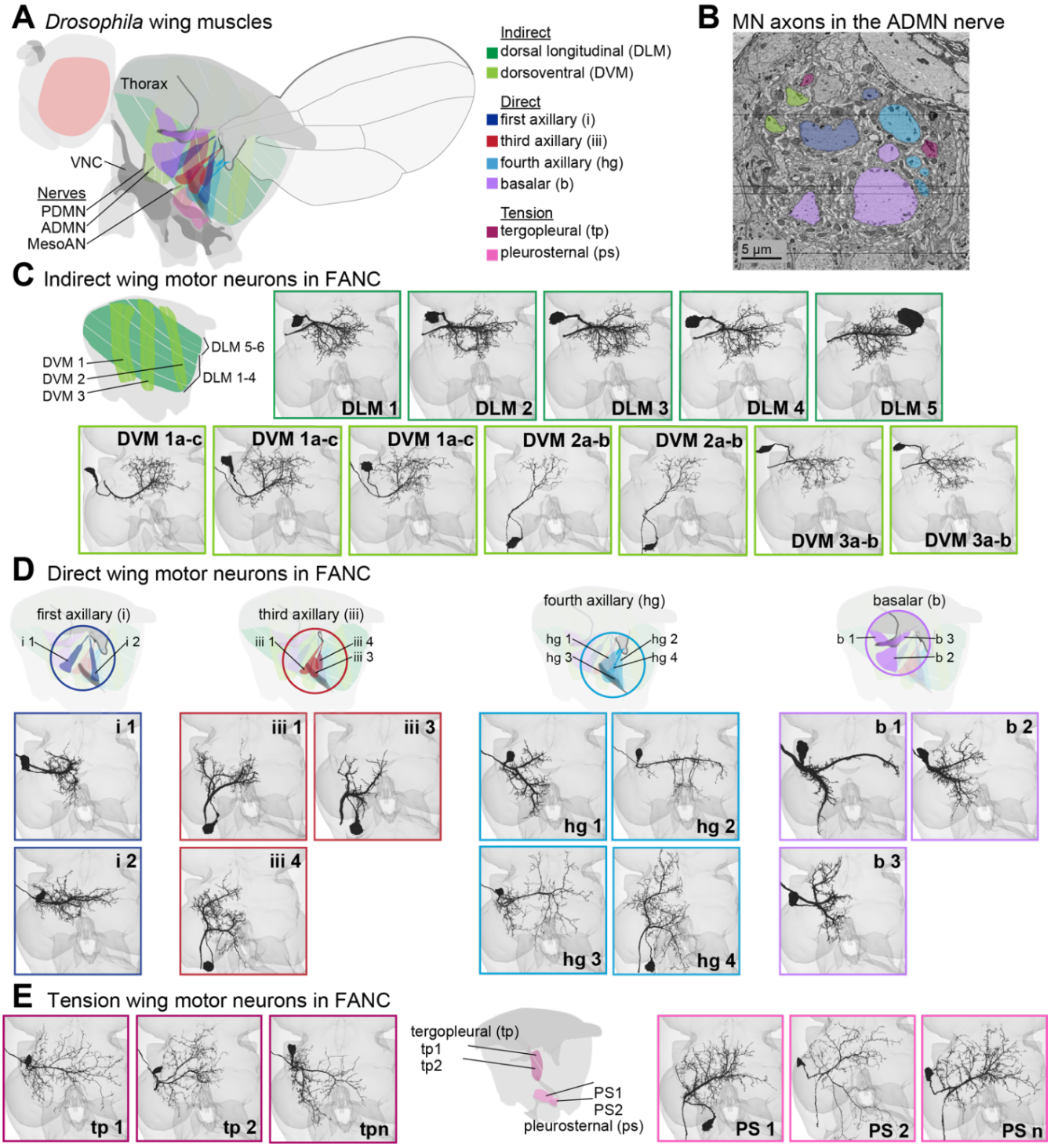

Figure 5. Identification of wing motor neurons (MNs) in FANC. (**A**) Cartoon showing muscles that power and finely control wing motion. Indirect power muscles (green) span the thorax along the anterior-posterior and dorsal-ventral axes; their antagonistic contractions resonate the thorax at high frequencies and cause the wings to move back and forth during flight. Direct muscles attach directly to sclerites within the wing hinge and finely adjust the wing motion. Tension muscles attach to the inner wall of the thorax and internal apodemes, and their contractions are thought to alter the tension of the thorax, thus modifying the oscillations generated by the indirect power muscles. Also pictured is the VNC, with the nerves that carry MN axons to wing muscles (PDMN, ADMN, MesoAN). (**B**) EM image from FANC showing a cross section of the ADMN nerve. MN axons are colored according to the key in **A**. MNs that innervate muscles with similar attachment points often fasciculate together in the nerve. Horizontal lines are due to missing slices from the serial-sectioned reconstructed volume. (**C**) Segmented and proofread MNs from FANC that innervate indirect MNs. We could not differentiate the MNs that innervate individual DVM fibers within each muscle (DVM 1, DVM 2, or DVM 3), so they share a common label (i.e. DVM 1a-c refers to all three MNs that innervate DVM 1). See methods for details on identification for **C-E**. (**D**) Segmented and proofread MNs from FANC that innervate direct muscles. (**E**) Segmented and proofread MNs from FANC that innervate tension muscles.

Identification of wing motor neurons (MNs)

We next focused our analysis on the wing motor system. The wing musculature (**Figure 5A**) can be broadly divided into three groups based on their functional roles in flight (Dickinson and Tu, 1997; Pringle, 1957). First, 13 large indirect muscle fibers power flight by causing the thorax to resonate at high frequencies and drive the wings to flap back and forth via their actions on the mechanically complex wing hinge (Deora et al., 2017). The 13 fibers are organized into 4 muscles, a single dorsal-longitudinal muscle (consisting of 6 fibers, DLM1-6), and three dorsoventral muscles (consisting of 3 fibers (DVM1), and 2 fibers (DVM2 and DVM3)). These muscles possess a distinct asynchronous physiology, in that each contraction is triggered by stretch and not by the arrival of an action potential in the presynaptic MN. Second, a set of 12 direct steering muscles can rapidly adjust wing motion via their insertions on hardened cuticle elements within the wing hinge called sclerites. Third, the lateral side of the thorax is equipped with 4 tension muscles, which although not directly connecting to the sclerites at the base of the wing, are thought to adjust wing motion via their effects on the mechanical stiffness of the thorax (Nachtigall and Wilson, 1967; Pringle, 1957). Both the direct steering muscles and tension muscles exhibit the more typical twitch-type physiology and morphology, in that each contraction is triggered by a motor spike and each muscle is composed of a large number of small fibers.

We identified the MNs that innervate wing muscles by locating neurons in FANC with cell bodies in the VNC and axons that leave through the motor fascicle of one of the three nerves associated with the wing neuropil: the anterior dorsal mesothoracic nerve (ADMN, **Figure 5B**), posterior dorsal mesothoracic nerve, and the mesothoracic accessory nerve (Court et al., 2020; Phelps et al., 2021). We found 37 neurons on each side, 33 of which we determined to be MNs (the other 4 are discussed below). We identified the same MNs on each side, but here we focus our analysis on the left side (direct MNs, links to other wing MNs in **Table S4**).

We identified the muscle targets of all the wing MNs in FANC. Most identifications were based on dendritic morphology alone. We relied on two landmark papers (O'Sullivan et al., 2018; Trimarchi and Schneiderman, 1994) and personal communication of work in progress (Erhardt, Whitehead, et al. and Cheong, Eichler et al., in preparation) to identify most of the direct and tension MNs (**Figure 5D-E**). We then identified all of the MNs that innervate indirect muscles (**Figure 5C**) and named them according to previously established conventions (Ikeda and Koenig, 1988; Schlurmann and Hausen, 2007).

As with the leg motor system, our analysis allowed us to make some noteworthy observations. The MNs of the DLMs were the only MNs we found to possess presynaptic sites in the VNC. This finding provides insight into a prior controversy as to whether the MNs of the DLMs constitute the CPG that is responsible for the low frequency spike rate that maintains the muscles in an active state, or whether the MNs simply follow the cyclic input of a premotor oscillator (Harcombe and Wyman, 1977; Koenig and Ikeda, 1983). These observations also complement recent work that suggests that gap junctions between DLM MNs function to offset their spike timing during flight (Hürkey et al., 2022).

We found four efferent neurons that we did not categorize as excitatory MNs. One is the previously described peripherally synapsing interneuron, which plays an important role in escape behavior (King and Wyman, 1980), and three are previously undescribed efferent neurons, one of which may be a spiracle MN. Another has a branch that ascends to the brain, and is presumably not a MN (**Figure S4**).

A neural circuit to retract the front legs during escape take-off.

With knowledge of the muscle targets of the front leg and wing MNs, the connectome points to clear hypotheses about the physiological and behavioral roles of many premotor neurons. We illustrate the potential of combining the VNC connectome and MN projectome with identification and analysis of premotor neurons that coordinate the fly's legs and wings during escape takeoff (**Figure 6A**).

Previous research identified a class of VNC local neurons (giant fiber coupled or GFC) that are electrically coupled to the giant fiber (Kennedy and Broadie, 2018), a massive descending neuron that drives evasive escape takeoff (Tanouye and Wyman, 1980; von Reyn et al., 2014). In the FANC volume, we found and proofread two subtypes of GFC interneurons (GFC2 and GFC4). We then used FANC synapse predictions to understand how they are connected onto leg and wing MNs (**Figure 6B**). The morphology of the GFC2 and GFC4 interneurons indicates that they develop from stem cell hemilineages (18B and 11A, respectively) that release the excitatory neurotransmitter acetylcholine (Lacin et al., 2019).

We found that the GFC2 interneurons synapse onto indirect and tension wing MNs as well as tergotrochanter (TT) MNs that innervate the middle leg (T2), consistent with previous literature (Tanouye and Wyman, 1980). In addition to its role in T2 trochanter-femur extension during jumping, the enormous TT muscle (which is a twitch-type fiber) is also thought to function in helping to quickly initiate the first cycle of mechanical oscillation in the power muscles that will maintain flight (Nachtigall and Wilson, 1967). Thus, GFC2 interneurons are positioned to excite MNs that drive two parallel motor programs: jumping and initiation of the flight motor. The other

interneuron subtype, GFC4, synapses onto front leg (T1) MNs that flex either the trochanter-femur (**Figure 3D-G)** or tibia. This connectivity suggests that descending input from the giant fiber drives synchronized extension of the middle legs (jumping) and flexion of the front legs (lift-off). Although the role of the T1 leg retraction during take-off has not been previously described, it is clearly visible in high-speed videos of *Drosophila* escape (Card and Dickinson, 2008; Trimarchi and Schneiderman, 1993; von Reyn et al., 2014).

GFC4 interneurons synapse exclusively on the largest trochanter and tibia flexor MNs (**Figure 6C**, **Figure 3F**). This is striking because leg MNs are typically recruited in a hierarchical sequence, from small, low-force-producing MNs to large, high-force-producing MNs (Azevedo et al., 2020). However, in paired electrophysiological recordings from tibia flexor MNs, we previously observed occasional violations of the recruitment order, in which MNs at the top of the hierarchy would fire before MNs at the bottom (Azevedo et al., 2020). We hypothesized that these violations could occur during escape behaviors, as was previously described in zebrafish (Menelaou and McLean, 2012). We now find that descending input from the giant fiber is positioned to subvert the standard leg MN recruitment order to drive rapid, ballistic escape behavior via the GFC4 interneurons.

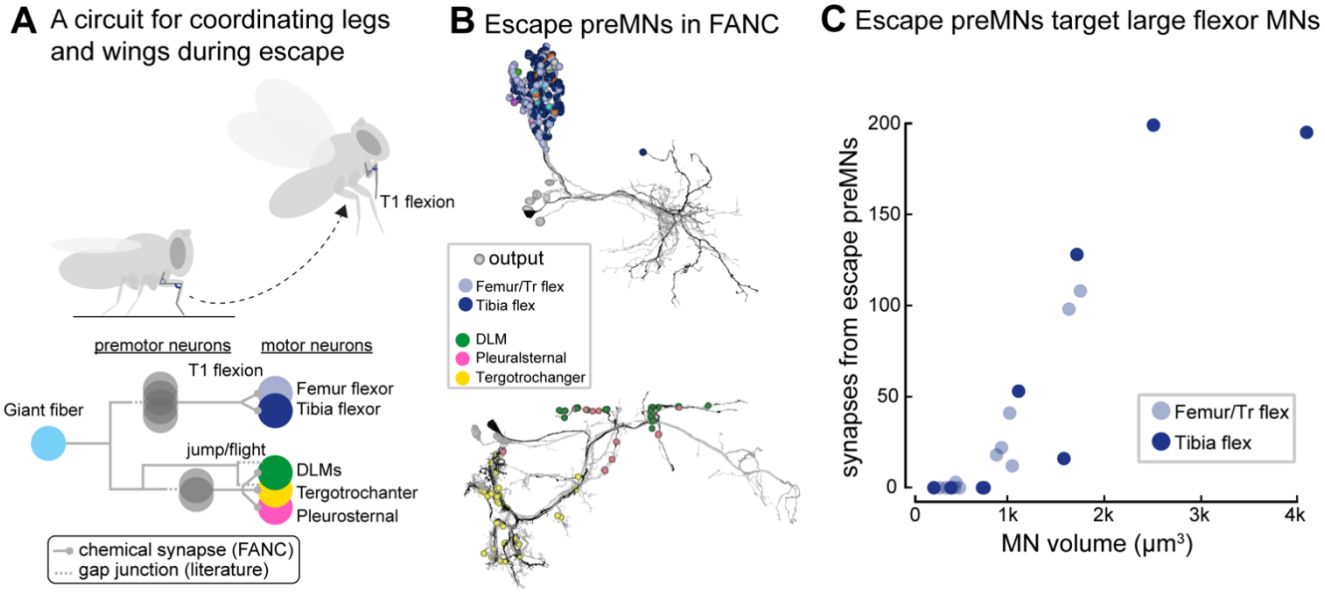

Figure 6. Circuits that coordinate the wings and legs during escape takeoff. (**A**) Schematic of a proposed circuit for escape based on prior literature and FANC synapse predictions. The Giant Fiber (GF) excites wing and middle (T2) leg MNs as well as premotor neurons (preMNs) through gap junctions. In FANC, preMNs that are electrically coupled to the GF target T1tibia and trochanter -femur flexor MNs as well as MNs that innervate T2 leg tergotrochanter muscles, DLMs, and thorax tension muscles (the pleurosternals). (**B**) We identified interneurons that have been previously shown to be electrically coupled to the giant fiber (Kennedy and Broadie, 2018). The interneurons make synapses (spheres) onto MNs that drive jumping in the T2 legs (yellow), flexion of the T1 legs (blue), and initiate the flight motor (green and pink). A single interneuron in each group is represented in black to show morphology. Additional colors in T1 indicate synapses onto MNs other than tibia and trochanter flexors. (**C**) Premotor neurons that are electrically coupled to the giant fiber exclusively target the largest MNs innervating tibia and trochanter-femur flexor muscles, suggesting that this circuit motif bypasses the recruitment hierarchy to execute the fast high-force movements necessary for escape.

Discussion

The utility of a connectome is that it reveals the synaptic connectivity of the neuronal cell types and circuits that give rise to animal behavior. While comprehensive connectomes have been mapped for small crawling animals like *C. elegans* (Cook et al., 2019) and the *Drosophila* larva (Winding et al., 2022), we currently lack a synapse-level wiring diagram of motor circuits for any limbed animal. Here, we provide a draft connectome of a female adult *Drosophila* VNC, a platform for proofreading the draft connectome to completion, and analysis of a circuit that coordinates the legs and wings during escape behavior.

We also built a comprehensive dataset of motor neuron (MN) anatomy by combining data from EM, X-ray nanotomography, light-level imaging of genetic driver lines, and past literature (Baek and Mann, 2009; Brierley et al., 2012; Enriquez et al., 2015; Kuan et al., 2020; Meissner et al., 2020; Phelps et al., 2021; Venkatasubramanian et al., 2019). We leveraged these results to identify the type of movement driven by each MN in the connectome, enabling analyses of how premotor circuits coordinate MN populations to produce natural behaviors.

All limbed organisms face similar challenges of maintaining posture to counteract gravity, navigating uneven terrain, and manipulating objects in the environment. Connectomic-driven discovery represents a paradigm shift for investigating these fundamental motor control problems. Previous work on the neural control of movement has attempted to link neural dynamics to motor output, in part to infer the connectivity and function of premotor networks (Kawai et al., 2015; Lindén et al., 2022; Sauerbrei et al., 2020; Shenoy et al., 2013; Vyas et al., 2020). A connectome allows one to work backwards from the MNs to identify premotor networks that coordinate specific patterns of muscle activation and inhibition. The fly VNC also provides a unique opportunity to investigate two different modes of limbed locomotion: walking and flight.

The community effort to comprehensively reconstruct neurons and measure synaptic connections within FANC is ongoing. Although we have only proofread a small fraction of the total FANC dataset, the automated reconstruction, proofreading environment, and analysis tools enable interactive inquiry into the neurobiology of the VNC, just as it has for the adult fly brain (Galili et al., 2022) and larval nervous system (Eschbach and Zlatic, 2020). Even before the connectome is complete, researchers can proofread subcircuits as a means of generating and falsifying hypotheses. Here, we provide an example of how the connectome can generate hypotheses about circuit and behavioral function by identifying premotor neurons that coordinate the legs and wings during escape takeoff (**Figure 6**). Using tools to match VNC neurons reconstructed in the EM volume with GAL4 lines imaged by light microscopy (**Figure S2**), it is then possible to test these hypotheses with *in vivo* recordings and manipulations of neural activity. Additional software tools exist to facilitate comparison of neuronal morphology and connectivity across individual animals and to bridge EM datasets (Bates et al., 2020; Plaza et al., 2022). Even with a single connectome, however, it is possible to gain insight into morphology and neural circuitry that differ between related species. For example, our reconstruction revealed independent control of the femur and trochanter leg segments, which were previously thought to be mechanically fused in *Drosophila* (Hartenstein, 2006).

Even with these tools, there exist many challenges to interpreting a synaptic wiring diagram (Bargmann and Marder, 2013). First, synapses can be either excitatory or inhibitory. Fortunately, VNC neurons develop from stem cell hemilineages that share identifiable morphological features as well as neurotransmitter identity (Lacin et al., 2019). Therefore, hemilineage identification of VNC cell types can identify candidate neurotransmitters, as we did for the escape circuitry (**Figure 6**). As done previously for the whole fly brain EM dataset, we are currently using hemilineage identities as ground-truth for training convolutional neural networks to predict neurotransmitter identity directly from the EM image data (Eckstein et al., 2020).

A second challenge is the inability to see electrical synapses or neuromodulatory sites in connectome datasets. The spatial resolution of all existing large connectomic datasets is insufficient to resolve gap junctions, which are known to play an important role in sensorimotor processing within the VNC (Agrawal et al., 2020; Chen et al., 2021; Tanouye and Wyman, 1980). It is also not currently possible to identify sites of neuromodulation, which are essential for flexible motor control (Howard et al., 2019). Because EM reconstruction provides a map of chemical synaptic transmission between neurons, physiological measurements will also be necessary to test for the effects of gap junctions and neuromodulators.

The FANC connectome will have many uses beyond the study of limb motor control. For example, it will enable the identification and analysis of neural circuits for descending modulation (Aymanns et al., 2022; Namiki et al., 2018), ascending communication with the brain (Chen et al., 2022), and sensory organs distributed across the fly limbs, thorax, and abdomen (Tuthill and Wilson, 2016). By creating a bridge between the VNC connectome and the body, the MN projectome will facilitate development and analysis of neuromechanical models for flexible motor control (Lobato-Rios et al., 2022). Finally, now that the connectome of the larval *Drosophila* nervous system is complete (Winding et al., 2022), it will become possible to compare the anatomy and connectivity of identified cell-types and circuits across developmental stages of the fly life cycle (Agrawal and Tuthill, 2022).

Acknowledgements

This work was supported by a Searle Scholar Award, a Klingenstein-Simons Fellowship, a Pew Biomedical Scholar Award, a McKnight Scholar Award, a Sloan Research Fellowship, the New York Stem Cell Foundation, and a UW Innovation Award to JCT; a Genise Goldenson Award to WAL; NIH U19NS104655 to JCT and MD; NIH R01MH117808 to JCT, WAL, and HSS. JCT is a New York Stem Cell Foundation – Robertson Investigator. We thank Rachel Wilson for financial support of SG during development of braincircuits.io (via U19NS104655 and R01NS129647 to RIW). We thank Richard Mann, Han Cheong, Erica Ehrhardt, Gwyneth Card, and Greg Jefferis for assistance with leg and wing MN identification.

Materials and Methods

EM Dataset Alignment, Segmentation, Proofreading, and Annotation

We refined the alignment of the FANC dataset using self-supervised convolutional neural networks (Popovych et al., 2022). We trained a CNN to identify knife marks that occurred during imaging. We then used CNNs to segment the dataset into neurons and fragments of neurons and to predict synapse locations (Macrina et al., 2021), excluding regions of the data with knife marks. We also used a CNN to predict pre and postsynaptic partners (Buhmann et al., 2021). The automated segmentation was ingested into the ChunkedGraph data structure (Dorkenwald et al., 2022). We then corrected errors in the segmentation through manual proofreading with Google's Neuroglancer interface (Maitin-Shepard et al., 2021).

We imported synapse and cell body predictions into the Connectome Annotation Versioning Engine (CAVE), so that the associated cell segmentation objects for each annotation would be dynamically updated during proofreading (Consortium et al., 2021). This system allowed us to query the up-to-date connectivity graph and associated metadata, such as cell-type annotations. A suite of tools we created for analysis of the FANC dataset are described in **Figure S2**.

To assess the quality of the FANC automated segmentation and synapse prediction, we manually traced and annotated synapses for a subset of leg MNs using CATMAID (Saalfeld et al., 2009).

Automatic detection of neuron nuclei

We used a 3D CNN to detect neuronal cell bodies (Mu et al., 2021). Our 3D CNN estimated the probability that a $64 \times 64 \times 45$ nm^3 voxel belonged to a nucleus (Lee et al., 2017). Training labels were generated by selecting automatically segmented nuclei from the cell segmentation. The probability map was thresholded at 0.7, connected component labels were generated, and centroid and size for each connected component were computed. Objects with size dimension below (1376 nm, 1376 nm, 1800 nm) for (x, y, z) were excluded, leaving 17,076 putative nuclei (**Figure 1F**).

In the automatic cell segmentation, the nucleus was frequently segmented as a separate object from the remainder of the cell. To assist with analysis, we merged the nucleus to its cell within the cell segmentation. For each object in the dedicated nucleus segmentation, we shifted the dedicated nucleus segment by one $68.8 \times 68.8 \times 45$ nm^3 voxel in every direction and identified the most frequent object within the cell segmentation to determine the associated cell. (**Figure 1G**).

Validation of the segmentation results

Even with the size threshold, we still found some glia and non-nucleus objects in the list of 17,076 putative neuronal nuclei. We manually inspected each nucleus and its associated cell, mainly based on its size, shape, and contrast. We categorized them into 14,679 neurons, 1,987 glia, and 410 false positives (1st quality check). We then ran another quality check with these 14,679 neurons, and found 14,639 neurons and 40 glia (2nd quality check). We also found 15 fragments of neuronal nuclei whose major parts were already detected and 3 glia within this 14,639 neurons (3rd quality check), which resulted in 14,621 neurons, 2,030 glia, and 410 false positives and 15 duplicated neurons (**Figure 1E, S1**).

Identification of leg motor neuron targets

The identification of leg motor neurons is described in detail in **Appendix A**, the atlas of FANC T1L MNs.

Identification of wing motor neurons

Unlike the leg, previous literature has already linked fly MN morphologies to muscle targets using muscle back-fills and specific Gal4 drivers (Ikeda and Koenig, 1988; O'Sullivan et al., 2018; Schlurmann and Hausen, 2007; Trimarchi and Schneiderman, 1994), so we were able to identify many of the neurons based on morphology alone. We identified wing and thorax MNs in FANC by finding neurons with cell bodies in the VNC and axons leaving through one of three wing-associated nerves: the anterior dorsal mesothoracic nerve (ADMN), posterior dorsal mesothoracic nerve (PDMN), and the mesothoracic accessory nerve (MesoAN; (Court et al., 2020). We found 37 neurons on each side. The right side MesoAN is partially severed (**Figure S3H**), so some of the MNs could not be reliably traced to a cell body. We only discuss the left side, but all neurons could be paired across the midline by eye. Of the 37 neurons, four were eliminated as wing and thorax MNs. One is the peripherally synapsing interneuron (King and Wyman, 1980), one may be a spiracle MN, and one has a branch that ascends to the brain. We categorized the wing and thorax MNs as indirect, direct, or tension, based on their proposed function (Dickinson and Tu, 1997). The three tergotrochanter (TT) MN axons travel through the PDMN (**Figure S4A**), but they innervate leg muscles, so we have not included them.

The indirect muscles contain two antagonistic groups: dorsal longitudinal muscles (DLMs) and dorsoventral muscles (DVMs). The six DLM fibers are innervated by five MNs (Ikeda and Koenig, 1988). We differentiated the first four DLMs based on the position of their axons along the anterior-posterior axis; DLM 5, which innervates muscle fibers five and six, is identifiable by its large contralateral cell body. It also has the posterior-most axon, so we labeled the DLM MN with the anterior-most axon as DLM 1. We found three MNs in the ADMN that innervate DVM 1, two MNs in the MesoAN that innervate DVM 2, and two MNs in the PDMN that innervate DVM 3, according to the morphologies and nomenclature established in *Calliphora* (Schlurmann and Hausen, 2007).

Unlike in the leg, direct wing muscles are innervated by a single MN (Heide, 1983). We relied on two papers to identify most of the direct MNs (Trimarchi and Schneiderman, 1994), and identified the rest based on morphology and fasciculation in FANC and

consultation with other experts in the field (Han Cheong, Erica Ehrhardt, personal communication). The first axillary (i) muscle i1 was identified from Trimarchi and Schneiderman; i2 is identified with low confidence due to its projection across the midline in FANC, which was not previously observed using light microscopy. It does, however, fasciculate with i1. The third axillary MNs iii1 and iii3 were identified from literature. We determined iii4 based on its similar morphology and fasciculation in the MesoAN. The fourth MN that looks similar to the iii MNs was determined to be hg4 (Han Cheong, personal communication). The fourth axillary MNs hg1 and hg2 were determined based on literature; hg3 was determined based on its similar morphology to hg2. hg2 and hg3 MNs have a similar morphology, so our confidence in their assignment is lower than other wing MNs. Basalar MNs b1 and b2 were identified from literature. We identified the third basalar MN b3 based on its fasciculation with MNs b1 and b2.

There are two sets of tension muscles, defined by the sclerites they attach to: the tergopleural (tp) muscles and the pleurosternal (ps) muscles. We identified tp1, tp2, and tpn from literature, although the morphologies we observed in FANC were not as similar for tergopleural MNs as other MNs. For the pleurosternal muscles, we found three candidate MNs instead of two (**Figure S3**).

The main tergotrochanter MN was identified based on previous literature (Bacon and Strausfeld, 1986). Two small MNs whose axons travel alongside the large tergotrochanter axon are predicted to either innervate the large TT muscle or innervate the intracoxal depressor and levator, respectively (muscles 67 and 68, according to (Miller, 1950)).

References Cited

Agrawal, S., Dickinson, E.S., Sustar, A., Gurung, P., Shepherd, D., Truman, J.W., Tuthill, J.C., 2020. Central processing of leg proprioception in Drosophila. eLife 9, e60299. https://doi.org/10.7554/eLife.60299

Agrawal, S., Tuthill, J.C., 2022. The two-body problem: Proprioception and motor control across the metamorphic divide. Curr. Opin. Neurobiol. 74, 102546. https://doi.org/10.1016/j.conb.2022.102546

Ampatzis, K., Song, J., Ausborn, J., Manira, A.E., 2013. Pattern of Innervation and Recruitment of Different Classes of Motoneurons in Adult Zebrafish. J. Neurosci. 33, 10875–10886. https://doi.org/10.1523/JNEUROSCI.0896-13.2013

Arber, S., 2012. Motor Circuits in Action: Specification, Connectivity, and Function. Neuron 74, 975–989. https://doi.org/10.1016/j.neuron.2012.05.011

Arber, S., Costa, R.M., 2022. Networking brainstem and basal ganglia circuits for movement. Nat. Rev. Neurosci. 23, 342–360. https://doi.org/10.1038/s41583-022-00581-w

Aymanns, F., Chen, C.-L., Ramdya, P., 2022. Descending neuron population dynamics during odor-evoked and spontaneous limb-dependent behaviors. eLife 11, e81527. https://doi.org/10.7554/eLife.81527

Azevedo, A.W., Dickinson, E.S., Gurung, P., Venkatasubramanian, L., Mann, R.S., Tuthill, J.C., 2020. A size principle for recruitment of Drosophila leg motor neurons. eLife 9, e56754. https://doi.org/10.7554/eLife.56754

Bacon, J.P., Strausfeld, N.J., 1986. The dipteran 'Giant fibre' pathway: neurons and signals. J. Comp. Physiol. A 158, 529–548. https://doi.org/10.1007/BF00603798

Baek, M., Mann, R.S., 2009. Lineage and Birth Date Specify Motor Neuron Targeting and Dendritic Architecture in Adult Drosophila. J. Neurosci. 29, 6904–6916. https://doi.org/10.1523/JNEUROSCI.1585-09.2009

Bargmann, C.I., Marder, E., 2013. From the connectome to brain function. Nat. Methods 10, 483–490. https://doi.org/10.1038/nmeth.2451

Bässler, U., Büschges, A., 1998. Pattern generation for stick insect walking movements - multisensory control of a locomotor program. Brain Res. Brain Res. Rev. 27, 65–88.

Bates, A.S., Manton, J.D., Jagannathan, S.R., Costa, M., Schlegel, P., Rohlfing, T., Jefferis, G.S., 2020. The natverse, a versatile toolbox for combining and analysing neuroanatomical data. eLife 9, e53350. https://doi.org/10.7554/eLife.53350

Binder, M.D., Powers, R.K., Heckman, C.J., 2020. Nonlinear Input-Output Functions of Motoneurons. Physiol. Bethesda Md 35, 31–39. https://doi.org/10.1152/physiol.00026.2019

Brierley, D. j., Rathore, K., VijayRaghavan, K., Williams, D. w., 2012. Developmental origins and architecture of Drosophila leg motoneurons. J. Comp. Neurol. 520, 1629–1649. https://doi.org/10.1002/cne.23003

Brown, M.C., Jansen, J.K., Van Essen, D., 1976. Polyneuronal innervation of skeletal muscle in new-born rats and its elimination during maturation. J. Physiol. 261, 387–422.

Buhmann, J., Sheridan, A., Gerhard, S., Krause, R., Nguyen, T., Heinrich, L., Schlegel, P., Lee, W.-C.A., Wilson, R., Saalfeld, S., Jefferis, G., Bock, D., Turaga, S., Cook, M., Funke, J., 2020. Automatic Detection of Synaptic Partners in a Whole-Brain Drosophila EM Dataset. https://doi.org/10.1101/2019.12.12.874172

Buhmann, J., Sheridan, A., Malin-Mayor, C., Schlegel, P., Gerhard, S., Kazimiers, T., Krause, R., Nguyen, T.M., Heinrich, L., Lee, W.-C.A., Wilson, R., Saalfeld, S., Jefferis, G.S.X.E., Bock, D.D., Turaga, S.C., Cook, M., Funke, J., 2021. Automatic detection of synaptic partners in a whole-brain Drosophila electron microscopy data set. Nat. Methods 18, 771–774. https://doi.org/10.1038/s41592-021-01183-7

Burke, R.E., 2011. Motor Units: Anatomy, Physiology, and Functional Organization, in: Comprehensive Physiology. John Wiley & Sons, Ltd, pp. 345–422. https://doi.org/10.1002/cphy.cp010210

Burrows, M., 1996. The Neurobiology of an Insect Brain. Oxford University Press, Oxford, New York.

Burrows, M., Horridge, G.A., 1974. The Organization of Inputs to Motoneurons of the Locust Metathoracic Leg. Philos. Trans. R. Soc. Lond. B. Biol. Sci. 269, 49–94.

Card, G., Dickinson, M., 2008. Performance trade-offs in the flight initiation of Drosophila. J. Exp. Biol. 211, 341–353. https://doi.org/10.1242/jeb.012682

Chen, C., Agrawal, S., Mark, B., Mamiya, A., Sustar, A., Phelps, J.S., Lee, W.-C.A., Dickson, B.J., Card, G.M., Tuthill, J.C., 2021. Functional architecture of neural circuits for leg proprioception in Drosophila. Curr. Biol. 31, 5163-5175.e7. https://doi.org/10.1016/j.cub.2021.09.035

Chen, C.-L., Aymanns, F., Minegishi, R., Matsuda, V.D.V., Talabot, N., Günel, S., Dickson, B.J., Ramdya, P., 2022. Ascending neurons convey behavioral state to integrative sensory and action selection centers in the brain. https://doi.org/10.1101/2022.02.09.479566

Consortium, Mic., Bae, J.A., Baptiste, M., Bodor, A.L., Brittain, D., Buchanan, J., Bumbarger, D.J., Castro, M.A., Celii, B., Cobos, E., Collman, F., Costa, N.M. da, Dorkenwald, S., Elabbady, L., Fahey, P.G., Fliss, T., Froudarakis, E., Gager, J., Gamlin, C., Halageri, A., Hebditch, J., Jia, Z., Jordan, C., Kapner, D., Kemnitz, N., Kinn, S., Koolman, S., Kuehner, K., Lee, K., Li, K., Lu, R., Macrina, T., Mahalingam, G., McReynolds, S., Miranda, E., Mitchell, E., Mondal, S.S., Moore, M., Mu, S., Muhammad, T., Nehoran, B., Ogedengbe, O., Papadopoulos, C., Papadopoulos, S., Patel, S., Pitkow, X., Popovych, S., Ramos, A., Reid, R.C., Reimer, J., Schneider-Mizell, C.M., Seung, H.S., Silverman, B., Silversmith, W., Sterling, A., Sinz, F.H., Smith, C.L., Suckow, S., Takeno, M., Tan, Z.H., Tolias, A.S., Torres, R., Turner, N.L., Walker, E.Y., Wang, T., Williams, G., Williams, S., Willie, K., Willie, R., Wong, W., Wu, J., Xu, C., Yang, R., Yatsenko, D., Ye, F., Yin, W., Yu, S., 2021. Functional connectomics spanning multiple areas of mouse visual cortex. https://doi.org/10.1101/2021.07.28.454025

Cook, S.J., Jarrell, T.A., Brittin, C.A., Wang, Y., Bloniarz, A.E., Yakovlev, M.A., Nguyen, K.C.Q., Tang, L.T.-H., Bayer, E.A., Duerr, J.S., Bülow, H.E., Hobert, O., Hall, D.H., Emmons, S.W., 2019. Whole-animal connectomes of both Caenorhabditis elegans sexes. Nature 571, 63–71. https://doi.org/10.1038/s41586-019-1352-7

Court, R., Namiki, S., Armstrong, J.D., Börner, J., Card, G., Costa, M., Dickinson, M., Duch, C., Korff, W., Mann, R., Merritt, D., Murphey, R.K., Seeds, A.M., Shirangi, T., Simpson, J.H., Truman, J.W., Tuthill, J.C., Williams, D.W., Shepherd, D., 2020. A Systematic Nomenclature for the Drosophila Ventral Nerve Cord. Neuron 107, 1071-1079.e2. https://doi.org/10.1016/j.neuron.2020.08.005

Deora, T., Gundiah, N., Sane, S.P., 2017. Mechanics of the thorax in flies. J. Exp. Biol. 220, 1382–1395. https://doi.org/10.1242/jeb.128363

Dickinson, M.H., Tu, M.S., 1997. The Function of Dipteran Flight Muscle. Comp. Biochem. Physiol. A Physiol. 116, 223–238. https://doi.org/10.1016/S0300-9629(96)00162-4

Dorkenwald, S., McKellar, C.E., Macrina, T., Kemnitz, N., Lee, K., Lu, R., Wu, J., Popovych, S., Mitchell, E., Nehoran, B., Jia, Z., Bae, J.A., Mu, S., Ih, D., Castro, M., Ogedengbe, O., Halageri, A., Kuehner, K., Sterling, A.R., Ashwood, Z., Zung, J., Brittain, D., Collman, F., Schneider-Mizell, C., Jordan, C., Silversmith, W., Baker, C., Deutsch, D., Encarnacion-Rivera, L., Kumar, S., Burke, A., Bland, D., Gager, J., Hebditch, J., Koolman, S., Moore, M., Morejohn, S., Silverman, B., Willie, K., Willie, R., Yu, S.-C., Murthy, M., Seung, H.S., 2022. FlyWire: online community for whole-brain connectomics. Nat. Methods 19, 119–128. https://doi.org/10.1038/s41592-021-01330-0

Eckstein, N., Bates, A.S., Du, M., Hartenstein, V., Jefferis, G.S.X.E., Funke, J., 2020. Neurotransmitter Classification from Electron Microscopy Images at Synaptic Sites in Drosophila. https://doi.org/10.1101/2020.06.12.148775

Enriquez, J., Venkatasubramanian, L., Baek, M., Peterson, M., Aghayeva, U., Mann, R.S., 2015. Specification of individual adult motor neuron morphologies by combinatorial transcription factor codes. Neuron 86, 955–970. https://doi.org/10.1016/j.neuron.2015.04.011

Eschbach, C., Zlatic, M., 2020. Useful road maps: studying Drosophila larva's central nervous system with the help of connectomics. Curr. Opin. Neurobiol. 65, 129–137. https://doi.org/10.1016/j.conb.2020.09.008

Galili, D.S., Jefferis, G.S.X.E., Costa, M., 2022. Connectomics and the neural basis of behaviour. Curr. Opin. Insect Sci. 100968. https://doi.org/10.1016/j.cois.2022.100968

Goulding, M., 2009. Circuits controlling vertebrate locomotion: moving in a new direction. Nat. Rev. Neurosci. 10, 507–518. https://doi.org/10.1038/nrn2608

Grillner, S., Kozlov, A., 2021. The CPGs for Limbed Locomotion-Facts and Fiction. Int. J. Mol. Sci. 22, 5882. https://doi.org/10.3390/ijms22115882

Harcombe, E.S., Wyman, R.J., 1977. Output pattern generation by Drosophila flight motoneurons. J. Neurophysiol. 40, 1066–1077. https://doi.org/10.1152/jn.1977.40.5.1066

Hartenstein, V., 2006. The Muscle Pattern of Drosophila, in: Sink, H. (Ed.), Muscle Development in Drosophila, Molecular Biology Intelligence Unit. Springer, New York, NY, pp. 8–27. https://doi.org/10.1007/0-387-32963-3_2

Heckman, C.J., Enoka, R.M., 2012. Motor unit. Compr. Physiol. 2, 2629–2682. https://doi.org/10.1002/cphy.c100087

Heide, G., 1983. Neural mechanisms of flight control in Diptera. BIONA-Rep. 2, 35–52.

Henneman, E., Olson, C.B., 1965. Relations between structure and function in the design of skeletal muscles. J. Neurophysiol. 28, 581–598. https://doi.org/10.1152/jn.1965.28.3.581

Henneman, E., Somjen, G., Carpenter, D.O., 1965a. Functional significance of cell size in spinal motoneurons. J. Neurophysiol. 28, 560–580. https://doi.org/10.1152/jn.1965.28.3.560

Henneman, E., Somjen, G., Carpenter, D.O., 1965b. Excitability and inhibitibility of motoneurons of different sizes. J. Neurophysiol. 28, 599–620. https://doi.org/10.1152/jn.1965.28.3.599

Hill, A.A.V., Cattaert, D., 2008. Recruitment in a heterogeneous population of motor neurons that innervates the depressor muscle of the crayfish walking leg muscle. J. Exp. Biol. 211, 613–629. https://doi.org/10.1242/jeb.006270

Howard, C.E., Chen, C.-L., Tabachnik, T., Hormigo, R., Ramdya, P., Mann, R.S., 2019. Serotonergic Modulation of Walking in Drosophila. Curr. Biol. CB 29, 4218-4230.e8. https://doi.org/10.1016/j.cub.2019.10.042

Hoyle, G., 1983. Muscles and their neural control. New York : Wiley.

Hulse, B.K., Haberkern, H., Franconville, R., Turner-Evans, D., Takemura, S., Wolff, T., Noorman, M., Dreher, M., Dan, C., Parekh, R., Hermundstad, A.M., Rubin, G.M., Jayaraman, V., 2021. A connectome of the Drosophila central complex reveals network motifs suitable for flexible navigation and context-dependent action selection. eLife 10, e66039. https://doi.org/10.7554/eLife.66039

Hürkey, S., Niemeyer, N., Schleimer, J.-H., Ryglewski, S., Schreiber, S., Duch, C., 2022. Insect asynchronous flight requires neural circuit de-synchronization by electrical synapses. https://doi.org/10.1101/2022.02.02.478622

Ikeda, K., Koenig, J.H., 1988. Morphological identification of the motor neurons innervating the dorsal longitudinal flight muscle of Drosophila melanogaster. J. Comp. Neurol. 273, 436–444. https://doi.org/10.1002/cne.902730312

Inagaki, H.K., Chen, S., Daie, K., Finkelstein, A., Fontolan, L., Romani, S., Svoboda, K., 2022. Neural Algorithms and Circuits for Motor Planning. Annu. Rev. Neurosci. 45, 249–271. https://doi.org/10.1146/annurev-neuro-092021-121730

Jenett, A., Rubin, G.M., Ngo, T.-T.B., Shepherd, D., Murphy, C., Dionne, H., Pfeiffer, B.D., Cavallaro, A., Hall, D., Jeter, J., Iyer, N., Fetter, D., Hausenfluck, J.H., Peng, H., Trautman, E.T., Svirskas, R.R., Myers, E.W., Iwinski, Z.R., Aso, Y., DePasquale, G.M., Enos, A., Hulamm, P., Lam, S.C.B., Li, H.-H., Laverty, T.R., Long, F., Qu, L., Murphy, S.D., Rokicki, K., Safford, T., Shaw, K., Simpson, J.H., Sowell, A., Tae, S., Yu, Y., Zugates, C.T., 2012. A GAL4-driver line resource for Drosophila neurobiology. Cell Rep. 2, 991–1001. https://doi.org/10.1016/j.celrep.2012.09.011

Karashchuk, P., Rupp, K.L., Dickinson, E.S., Walling-Bell, S., Sanders, E., Azim, E., Brunton, B.W., Tuthill, J.C., 2021. Anipose: A toolkit for robust markerless 3D pose estimation. Cell Rep. 36, 109730. https://doi.org/10.1016/j.celrep.2021.109730

Kasthuri, N., Lichtman, J.W., 2007. The rise of the "projectome." Nat. Methods 4, 307–308. https://doi.org/10.1038/nmeth0407-307

Kawai, R., Markman, T., Poddar, R., Ko, R., Fantana, A.L., Dhawale, A.K., Kampff, A.R., Ölveczky, B.P., 2015. Motor cortex is required for learning but not for executing a motor skill. Neuron 86, 800–812. https://doi.org/10.1016/j.neuron.2015.03.024

Kennedy, T., Broadie, K., 2018. Newly Identified Electrically Coupled Neurons Support Development of the Drosophila Giant Fiber Model Circuit. eNeuro 5, ENEURO.0346-18.2018. https://doi.org/10.1523/ENEURO.0346-18.2018

Kernell, D., 2006. The Motoneurone and its Muscle Fibres. Oxford University Press.

Kiehn, O., 2016. Decoding the organization of spinal circuits that control locomotion. Nat. Rev. Neurosci. 17, 224–238. https://doi.org/10.1038/nrn.2016.9

King, D.G., Wyman, R.J., 1980. Anatomy of the giant fibre pathway in Drosophila. I. Three thoracic components of the pathway. J. Neurocytol. 9, 753–770. https://doi.org/10.1007/BF01205017

Koenig, J.H., Ikeda, K., 1983. Reciprocal excitation between identified flight motor neurons inDrosophila and its effect on pattern generation. J. Comp. Physiol. 150, 305–317. https://doi.org/10.1007/BF00605020

Kuan, A.T., Phelps, J.S., Thomas, L.A., Nguyen, T.M., Han, J., Chen, C.-L., Azevedo, A.W., Tuthill, J.C., Funke, J., Cloetens, P., Pacureanu, A., Lee, W.-C.A., 2020. Dense neuronal reconstruction through X-ray holographic nano-tomography. Nat. Neurosci. 23, 1637–1643. https://doi.org/10.1038/s41593-020-0704-9

Lacin, H., Chen, H.-M., Long, X., Singer, R.H., Lee, T., Truman, J.W., 2019. Neurotransmitter identity is acquired in a lineage-restricted manner in the Drosophila CNS. eLife 8. https://doi.org/10.7554/eLife.43701

Lee, K., Zung, J., Li, P., Jain, V., Seung, H.S., 2017. Superhuman Accuracy on the SNEMI3D Connectomics Challenge. https://doi.org/10.48550/arXiv.1706.00120

Leiras, R., Cregg, J.M., Kiehn, O., 2022. Brainstem Circuits for Locomotion. Annu. Rev. Neurosci. 45, 63–85. https://doi.org/10.1146/annurev-neuro-082321-025137

Lindén, H., Petersen, P.C., Vestergaard, M., Berg, R.W., 2022. Movement is governed by rotational neural dynamics in spinal motor networks. Nature 610, 526–531. https://doi.org/10.1038/s41586-022-05293-w

Lobato-Rios, V., Ramalingasetty, S.T., Özdil, P.G., Arreguit, J., Ijspeert, A.J., Ramdya, P., 2022. NeuroMechFly, a neuromechanical model of adult Drosophila melanogaster. Nat. Methods 19, 620–627. https://doi.org/10.1038/s41592-022-01466-7

Macrina, T., Lee, K., Lu, R., Turner, N.L., Wu, J., Popovych, S., Silversmith, W., Kemnitz, N., Bae, J.A., Castro, M.A., Dorkenwald, S., Halageri, A., Jia, Z., Jordan, C., Li, K., Mitchell, E., Mondal, S.S., Mu, S., Nehoran, B., Wong, W., Yu, S., Bodor, A.L., Brittain, D., Buchanan, J., Bumbarger, D.J., Cobos, E., Collman, F., Elabbady, L., Fahey, P.G., Froudarakis, E., Kapner, D., Kinn, S., Mahalingam, G., Papadopoulos, S., Patel, S., Schneider-Mizell, C.M., Sinz, F.H., Takeno, M., Torres, R., Yin, W., Pitkow, X., Reimer, J., Tolias, A.S., Reid, R.C., Costa, N.M. da, Seung, H.S., 2021. Petascale neural circuit reconstruction: automated methods. https://doi.org/10.1101/2021.08.04.455162

Maitin-Shepard, J., Baden, A., Silversmith, W., Perlman, E., Collman, F., Blakely, T., Funke, J., Jordan, C., Falk, B., Kemnitz, N., tingzhao, Roat, C., Castro, M., Jagannathan, S., moenigin, Clements, J., Hoag, A., Katz, B., Parsons, D., Wu, J., Kamentsky, L., Chervakov, P., Hubbard, P., Berg, S., Hoffer, J., Halageri, A., Machacek, C., Mader, K., Roeder, L., Li, P.H., 2021. google/neuroglancer: https://doi.org/10.5281/zenodo.5573294

Manuel, M., Chardon, M., Tysseling, V., Heckman, C.J., 2019. Scaling of Motor Output, From Mouse to Humans. Physiology 34, 5–13. https://doi.org/10.1152/physiol.00021.2018

Mark, B., Lai, S.-L., Zarin, A.A., Manning, L., Pollington, H.Q., Litwin-Kumar, A., Cardona, A., Truman, J.W., Doe, C.Q., 2021. A developmental framework linking neurogenesis and circuit formation in the Drosophila CNS [WWW Document]. eLife. https://doi.org/10.7554/eLife.67510

Mcphedran, A.M., Wuerker, R.B., Henneman, E., 1965. Properties of motor units in a homogeneous red muscle (soleus) of the cat. J. Neurophysiol. 28, 71–84. https://doi.org/10.1152/jn.1965.28.1.71

Meissner, G.W., Dorman, Z., Nern, A., Forster, K., Gibney, T., Jeter, J., Johnson, L., He, Y., Lee, K., Melton, B., Yarbrough, B., Clements, J., Goina, C., Otsuna, H., Rokicki, K., Svirskas, R.R., Aso, Y., Card, G.M., Dickson, B.J., Ehrhardt, E., Goldammer, J., Ito, M., Korff, W., Minegishi, R., Namiki, S., Rubin, G.M., Sterne, G., Wolff, T., Malkesman, O., Team, F.P., 2020. An image resource of subdivided Drosophila GAL4-driver expression patterns for neuron-level searches. https://doi.org/10.1101/2020.05.29.080473

Menelaou, E., McLean, D.L., 2012. A gradient in endogenous rhythmicity and oscillatory drive matches recruitment order in an axial motor pool. J. Neurosci. Off. J. Soc. Neurosci. 32, 10925–10939. https://doi.org/10.1523/JNEUROSCI.1809-12.2012

Miller, A., 1950. The internal anatomy and histology of the imago of Drosophila melanogaster. Biol. Drosoph. 420–534.

Mu, S., Yu, S., Turner, N.L., McKellar, C.E., Dorkenwald, S., Collman, F., Koolman, S., Moore, M., Morejohn, S., Silverman, B., Willie, K., Willie, R., Bland, D., Burke, A., Ashwood, Z., Luther, K., Castro, M., Ogedengbe, O., Silversmith, W., Wu, J., Halageri, A., Macrina, T., Kemnitz, N., Murthy, M., Seung, H.S., 2021. 3D reconstruction of cell nuclei in a full Drosophila brain. https://doi.org/10.1101/2021.11.04.467197

Nachtigall, W., Wilson, D.M., 1967. Neuro-Muscular Control of Dipteran Flight. J. Exp. Biol. 47, 77–97. https://doi.org/10.1242/jeb.47.1.77

Namiki, S., Dickinson, M.H., Wong, A.M., Korff, W., Card, G.M., 2018. The functional organization of descending sensory-motor pathways in Drosophila. eLife 7, 1-50.e34272. https://doi.org/10.7554/eLife.34272

Nern, A., Pfeiffer, B.D., Rubin, G.M., 2015. Optimized tools for multicolor stochastic labeling reveal diverse stereotyped cell arrangements in the fly visual system. Proc. Natl. Acad. Sci. U. S. A. 112, E2967-2976. https://doi.org/10.1073/pnas.1506763112

O'Sullivan, A., Lindsay, T., Prudnikova, A., Erdi, B., Dickinson, M., von Philipsborn, A.C., 2018. Multifunctional Wing Motor Control of Song and Flight. Curr. Biol. CB 28, 2705-2717.e4. https://doi.org/10.1016/j.cub.2018.06.038

Otsuna, H., Ito, M., Kawase, T., 2018. Color depth MIP mask search: a new tool to expedite Split-GAL4 creation. bioRxiv 318006. https://doi.org/10.1101/318006

Phelps, J.S., Hildebrand, D.G.C., Graham, B.J., Kuan, A.T., Thomas, L.A., Nguyen, T.M., Buhmann, J., Azevedo, A.W., Sustar, A., Agrawal, S., Liu, M., Shanny, B.L., Funke, J., Tuthill, J.C., Lee, W.-C.A., 2021. Reconstruction of motor control circuits in adult Drosophila using automated transmission electron microscopy. Cell 184, 759-774.e18. https://doi.org/10.1016/j.cell.2020.12.013

Plaza, S.M., Clements, J., Dolafi, T., Umayam, L., Neubarth, N.N., Scheffer, L.K., Berg, S., 2022. neuPrint: An open access tool for EM connectomics. Front. Neuroinformatics 16, 896292. https://doi.org/10.3389/fninf.2022.896292

Popovych, S., Macrina, T., Kemnitz, N., Castro, M., Nehoran, B., Jia, Z., Bae, J.A., Mitchell, E., Mu, S., Trautman, E.T., Saalfeld, S., Li, K., Seung, S., 2022. Petascale pipeline for precise alignment of images from serial section electron microscopy. https://doi.org/10.1101/2022.03.25.485816

Pringle, J.W.S., 1957. Insect Flight. Cambridge University Press.

R. E. Snodgrass, 1935. Principles Of Insect Morphology.

Radnikow, G., Bässler, U., 1991. Function of a Muscle Whose Apodeme Travels Through a Joint Moved by Other Muscles: Why the Retractor Unguis Muscle in Stick Insects is Tripartite and has no Antagonist. J. Exp. Biol. 157, 87–99. https://doi.org/10.1242/jeb.157.1.87

Ruder, L., Arber, S., 2019. Brainstem Circuits Controlling Action Diversification. Annu. Rev. Neurosci. 42, 485–504. https://doi.org/10.1146/annurev-neuro-070918-050201

Rybak, I.A., Dougherty, K.J., Shevtsova, N.A., 2015. Organization of the Mammalian Locomotor CPG: Review of Computational Model and Circuit Architectures Based on Genetically Identified Spinal Interneurons. eNeuro 2, ENEURO.0069-15.2015. https://doi.org/10.1523/ENEURO.0069-15.2015

Saalfeld, S., Cardona, A., Hartenstein, V., Tomančák, P., 2009. CATMAID: collaborative annotation toolkit for massive amounts of image data. Bioinformatics 25, 1984–1986. https://doi.org/10.1093/bioinformatics/btp266

Sauerbrei, B.A., Guo, J.-Z., Cohen, J.D., Mischiati, M., Guo, W., Kabra, M., Verma, N., Mensh, B., Branson, K., Hantman, A.W., 2020. Cortical pattern generation during dexterous movement is input-driven. Nature 577, 386–391. https://doi.org/10.1038/s41586-019-1869-9

Schlurmann, M., Hausen, K., 2007. Motoneurons of the flight power muscles of the blowfly Calliphora erythrocephala: Structures and mutual dye coupling. J. Comp. Neurol. 500, 448–464. https://doi.org/10.1002/cne.21182

Schneider-Mizell, C.M., Gerhard, S., Longair, M., Kazimiers, T., Li, F., Zwart, M.F., Champion, A., Midgley, F.M., Fetter, R.D., Saalfeld, S., Cardona, A., 2016. Quantitative neuroanatomy for connectomics in Drosophila. eLife 5, e12059. https://doi.org/10.7554/eLife.12059

Shenoy, K.V., Sahani, M., Churchland, M.M., 2013. Cortical control of arm movements: a dynamical systems perspective. Annu. Rev. Neurosci. 36, 337–359. https://doi.org/10.1146/annurev-neuro-062111-150509

Siegler, M.V., 1982. Electrical coupling between supernumerary motor neurones in the locust. J. Exp. Biol. 101, 105–119. https://doi.org/10.1242/jeb.101.1.105

Tanouye, M.A., Wyman, R.J., 1980. Motor outputs of giant nerve fiber in Drosophila. J. Neurophysiol. 44, 405–421. https://doi.org/10.1152/jn.1980.44.2.405

Trimarchi, J.R., Schneiderman, A.M., 1994. The motor neurons innervating the direct flight muscles of Drosophila melanogaster are morphologically specialized. J. Comp. Neurol. 340, 427–443. https://doi.org/10.1002/cne.903400311

Trimarchi, J.R., Schneiderman, A.M., 1993. Giant fiber activation of an intrinsic muscle in the mesothoracic leg of Drosophila melanogaster. J. Exp. Biol. 177, 149–167. https://doi.org/10.1242/jeb.177.1.149

Tuthill, J.C., Wilson, R.I., 2016. Mechanosensation and Adaptive Motor Control in Insects. Curr. Biol. CB 26, R1022–R1038. https://doi.org/10.1016/j.cub.2016.06.070

Venkatasubramanian, L., Guo, Z., Xu, S., Tan, L., Xiao, Q., Nagarkar-Jaiswal, S., Mann, R.S., 2019. Stereotyped terminal axon branching of leg motor neurons mediated by IgSF proteins DIP-α and Dpr10. eLife 8. https://doi.org/10.7554/eLife.42692

von Reyn, C.R., Breads, P., Peek, M.Y., Zheng, G.Z., Williamson, W.R., Yee, A.L., Leonardo, A., Card, G.M., 2014. A spike-timing mechanism for action selection. Nat. Neurosci. 17, 962–970. https://doi.org/10.1038/nn.3741

Vyas, S., Golub, M.D., Sussillo, D., Shenoy, K.V., 2020. Computation Through Neural Population Dynamics. Annu. Rev. Neurosci. 43, 249–275. https://doi.org/10.1146/annurev-neuro-092619-094115

Winding, M., Pedigo, B.D., Barnes, C.L., Patsolic, H.G., Park, Y., Kazimiers, T., Fushiki, A., Andrade, I.V., Li, F., Valdes-Aleman, J., Khandelwal, A., Randel, N., Barsotti, E., Correia, A., Fetter, R.D., Hartenstein, V., Priebe, C.E., Vogelstein, J.T., Cardona, A., Zlatic, M., 2022. The connectome of an insect brain. https://doi.org/10.1101/2022.11.28.516756

Wolf, H., 2014. Inhibitory motoneurons in arthropod motor control: organisation, function, evolution. J. Comp. Physiol. A 200, 693–710. https://doi.org/10.1007/s00359-014-0922-2

Wuerker, R.B., McPhedran, A.M., Henneman, E., 1965. Properties of motor units in a heterogeneous pale muscle (m. gastrocnemius) of the cat. J. Neurophysiol. 28, 85–99. https://doi.org/10.1152/jn.1965.28.1.85

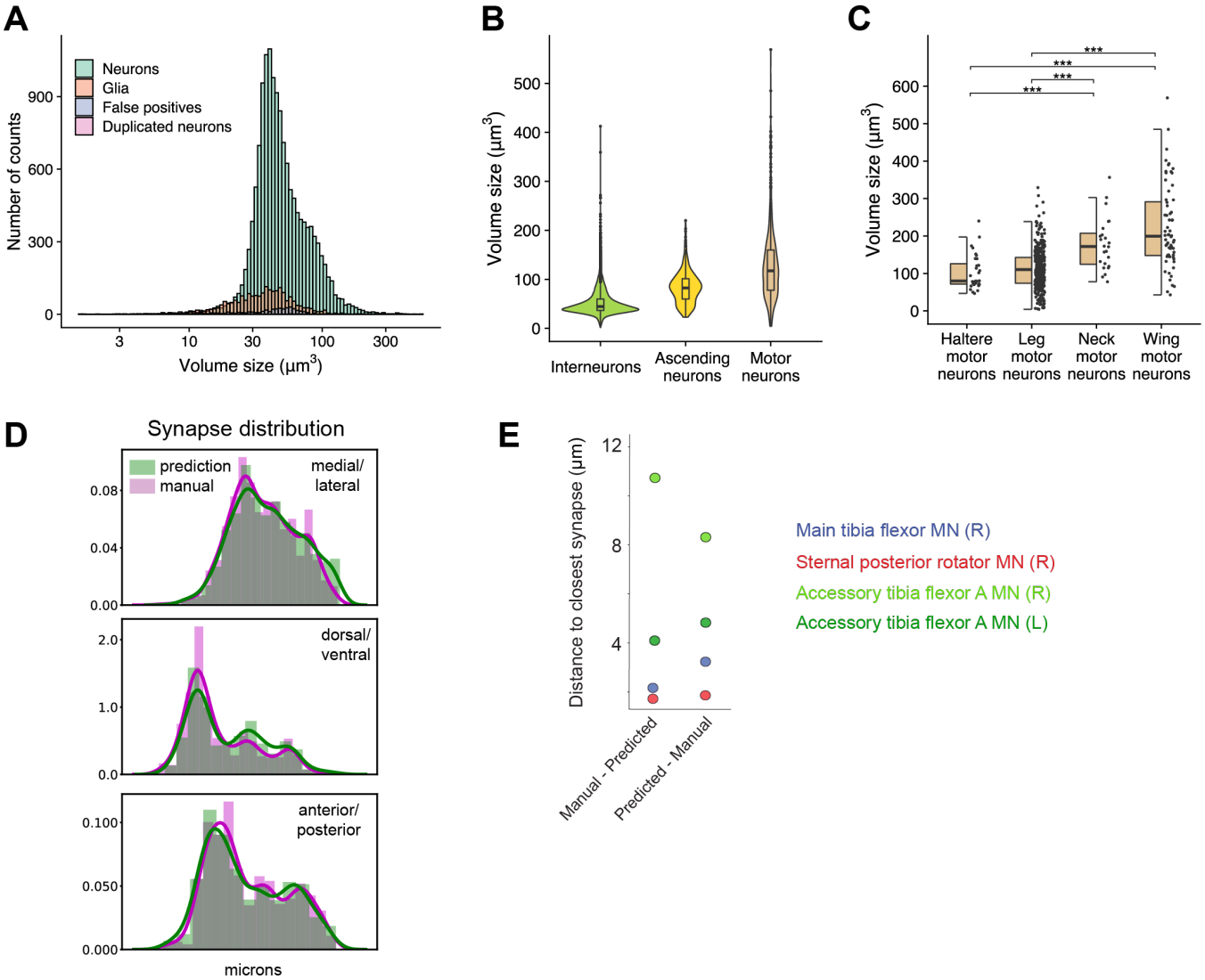

Figure S1. Additional quantification of FANC segmentation and synapse prediction. (**A**) Size distribution of all 17,076 putative nuclei. We manually inspected each putative nucleus and found 14621 neurons (85.6%), 2030 glia (11.9%), 410 false positives (2.4%), and 15 fragments of neuron nuclei detected twice (Duplicated neurons, 0.1%). Volume size is calculated based on the number of voxels within each detected objects. (**B**) Violin plot showing the size distribution of three major neuronal cell types that have cell bodies in VNC: interneurons (n=12,468), ascending neurons (n=1,668), and motor neurons (n=485). ($\chi 2$=1760.7, p<0.001, Kruskal-Wallis test.) VNC neurons with arbors projecting to the neck connective were labeled as ascending neurons. Motor neurons include haltere motor neurons (n=32), leg motor neurons (all T1, T2, and T3, n=371), neck motor neurons (n=24), and wing motor neurons (ADMN, PDMN, and MesoAN, n=58). Haltere, leg, and neck motor neurons were identified based on their skeleton nodes previously reported in CATMAID (Phelps et al., 2021). (**C**) Comparison of volume size between four motor neurons: haltere motor neurons, leg motor neurons, neck motor neurons, wing motor neurons. ($\chi 2$=84.816, p<0.001, Kruskal-Wallis test, ***p<0.001, post-hoc Benjamini–Hochberg procedure-corrected Dunn's test for multiple comparisons.) (**D**) Comparison of segmented cable using automated and manual reconstruction along all three spatial axes for the sternal posterior rotator motor neuron shown in Figure 2B. (**E**) Average distance between manual and automated synapse prediction for input synapses to the four manually reconstructed MNs.

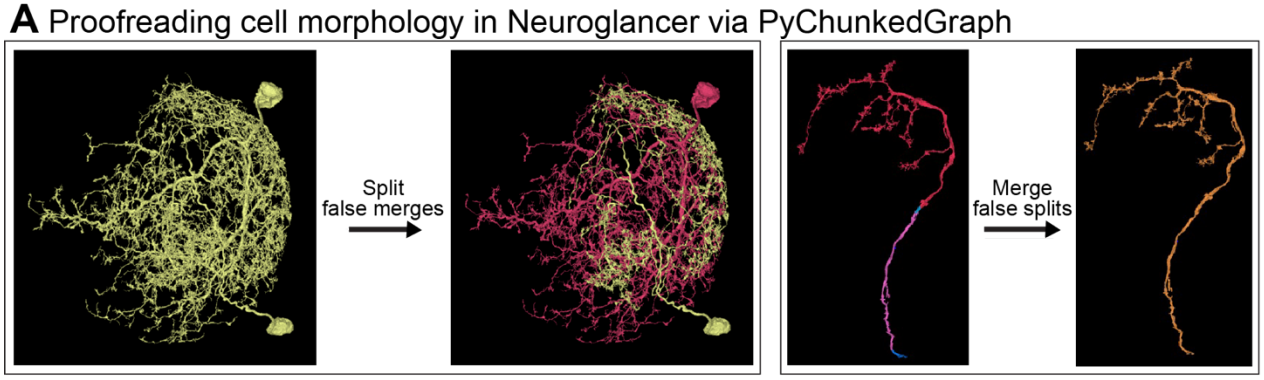

Figure S2. Summary of FANC software tools for cell proofreading: (**A**) Proofreading of cell morphology in Neuroglancer via PyChunkedGraph, (**B**) cell type annotation (**C**) identification, (**D**) cellular and circuit analysis, and (**E**) identification of genetic driver lines.

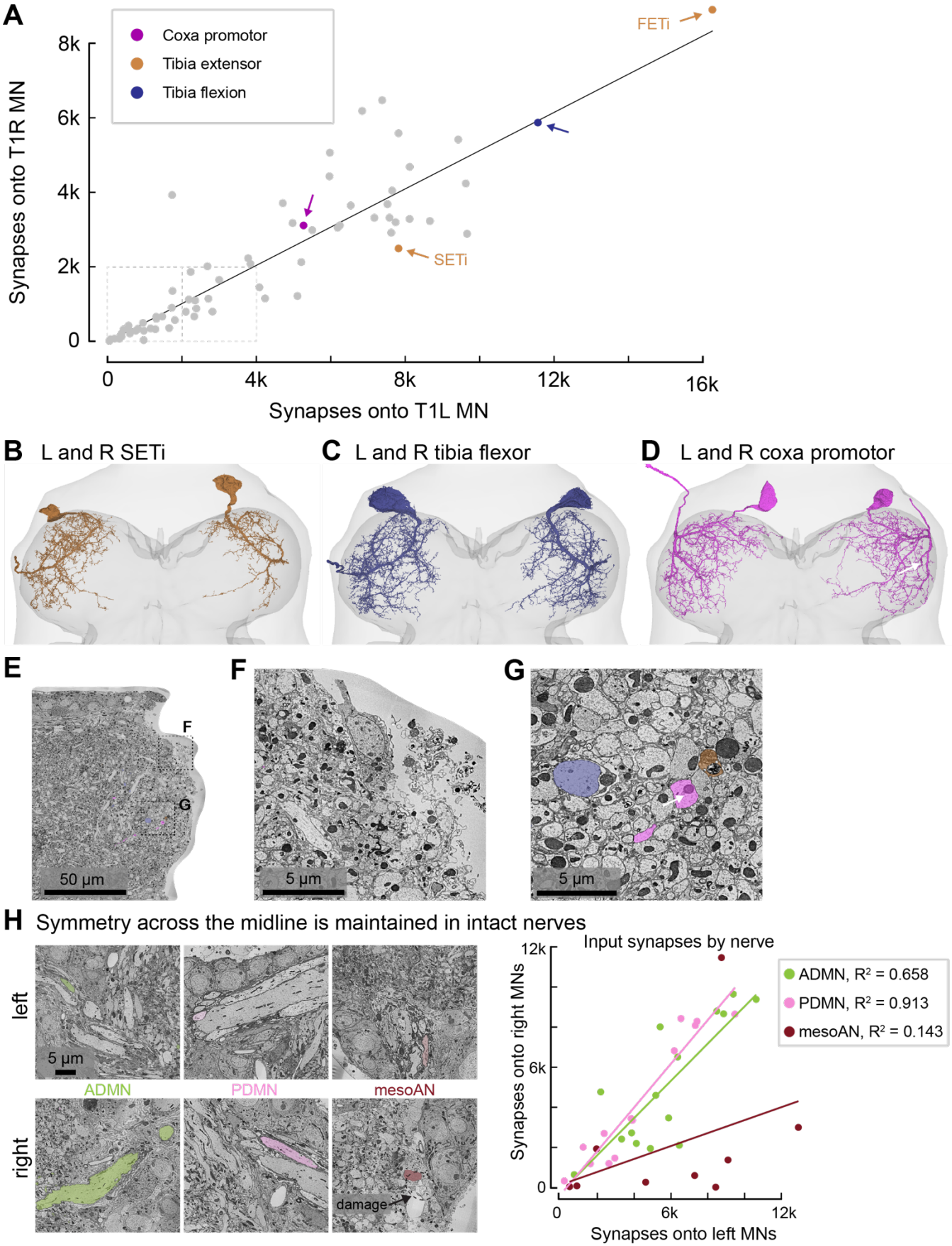

Figure S3. MNs in T1R have half as many input sites as MNs in T1L, likely due to rough dissection of the right T1 leg nerves. (**A**) The number of synapses onto the right T1 MN (y-axis) vs. onto the paired left T1 MN (x-axis). Colors indicate MN pairs in B-D. The slope of the relationship is 0.51, with a Pearson's correlation coefficient of 0.89, $p<10^{-22}$. (**B**) Left and right SETi MNs. The T1R neurons tend to appear smoother, with fewer fine twigs. (**C**) Left and right main tibia flexor MNs (Fast flexor, (Azevedo et al., 2020). (**D**) Left and right pleural coxa promotor MNs. Even though the axons exit the PrDN, rather than the ProLN, many of the dendrites of the T1R neuron run through the damaged regions. Blebby boutons can be seen (white arrow). (**E**) EM image of the damaged area of T1R. (**F**) Magnified view of the damaged area. (**G**) Magnified view of branches of MNs (colors) near the damaged area, including a bleb (arrow) in the pleural promotor MN (magenta). The bleb diameter is on the order of the primary neurite of the largest cell in the T1 neuromeres (blue). (**H**) For comparison, the right side mesoAN is clearly damaged while the right side ADMN and PDMN are intact. Left and right pairs of wing MNs in the ADMN and PDMN have similar numbers of postsynaptic sites, but the right side mesoAN MNs have fewer synapses than the left side mesoAN MNs.

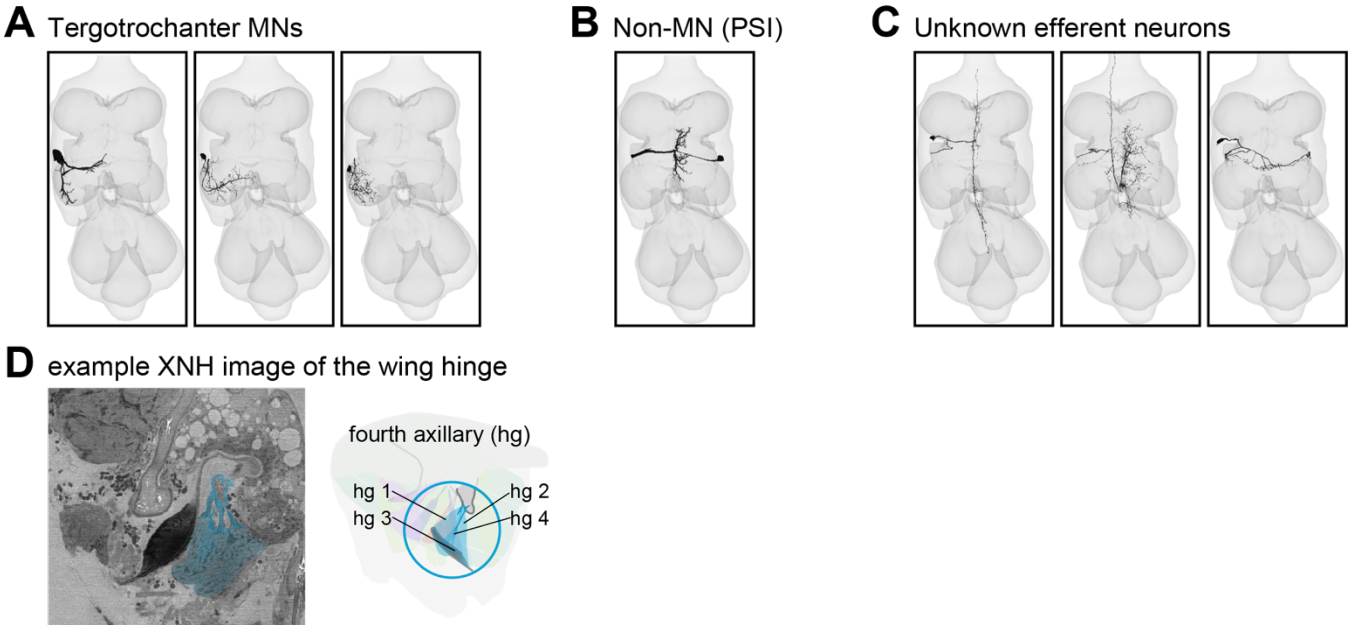

Figure S4. FANC efferent neurons with axons in the ADMN and PDMN that are not wing MNs. (**A**) MNs that innervate the T2 tergotrochanter leg muscle send axons through the PDMN. The two small neurons have not been identified previously. We identify them as TT MNs here based on their fasciculation with the main TT MN. We predict that they also innervate the main TT muscle, or the intracoxal depressor and levator, respectively (muscles 67 and 68 according to (Miller, A., 1950). (**B**) The peripherally synapsing interneuron (PSI) sends an axon into the PDMN but does not innervate muscles (King and Wyman, 1980). (**C**) Three other unidentified neurons have axons in the ADMN (unk1) or PDMN (PDMN). Their dendrites are thinner than any other motor neurons, and not like anything previously shown using light microscopy. Unk2 has an ascending process and its axon does not appear to travel all the way through the PDMN so it is not a MN. Unk3 may be a spiracle MN, as it slightly resembles the T1 spiracle MNs (Phelps et al., 2021). (**D**) A newly-collected XNH dataset of the wing and wing hinge was used to help inform the anatomical cartoon schematics.

Table S4. FANC Links to wing motor neurons

Indirect muscles		
Nerve	**Muscle**	
PDMN	DLM_1	link
PDMN	DLM_2	link
PDMN	DLM_3	link
PDMN	DLM_4	link
PDMN	DLM_5	link
ADMN	DVM_1a	link
ADMN	DVM_1b	link
ADMN	DVM_1c	link
mesoAN	DVM_2a	link
mesoAN	DVM_2b	link
PDMN	DVM_3a	link
PDMN	DVM_3b	link

Tension muscles		
Nerve	**Muscle**	
ADMN	tp1	link
ADMN	tp2	link
ADMN	tpn	link
mesoAN	PS1	link
mesoAN	PS2	link
mesoAN	PSn	link

Direct muscles		
Nerve	**Muscle**	
ADMN	i1	link
ADMN	i2	link
mesoAN	iii1	link
mesoAN	iii3	link
mesoAN	iii4	link
ADMN	hg1	link
ADMN	hg2	link
ADMN	hg3	link
mesoAN	hg4	link
ADMN	b1	link
ADMN	b2	link
ADMN	b3	link

Middle leg muscles / non motor neurons		
Nerve	**Muscle**	
PDMN	tt	link
PDMN	ttb	link
PDMN	ttc	link
PDMN	nonMN_PSI	link
PDMN	nonMN_unk1	link
PDMN	nonMN_unk2	link
ADMN	nonMN_unk3	link

Table S5. FANC links to leg motor neurons

nerve	segment	function	muscle	MNs	
DProN	thorax	swing	tergopleural promotor, pleural promotor	4	link
VProN	thorax	swing	sternal anterior rotator	2	link
ProAN	thorax	swing	sternal adductor	1	link
ProAN	thorax	stance	pleural remotor and abductor	2	link
ProAN	thorax	stance	sternal posterior rotator	4	link
Ventral	thorax	extend	tergotrochanter	4	link
Ventral	thorax	extend	sternotrochanter extensor	2	link
ProLN	coxa	extend	trochanter extensor	2	link
ProAN, VProN	coxa	flex	trochanter flexor	8	link
ProLN	coxa	flex	accessory trochanter flexor	3	link
ProLN	trochanter	reductor	femur reductor	6	link
ProLN	femur	extend	tibia extensor	2	link
ProLN	femur	flex	main tibia flexor	5	link
ProLN	femur	flex	accessory tibia flexor	10	link
ProLN	ltm	claw	long tendon muscle	8	link
ProLN	tibia	flex	tarsus depressor	2	link
ProLN	tibia	unknown	tarsus unidentified	4	link